

Particle Physics at the High Energy Frontier: The Fermilab Collider Experiments

Joseph R. Incandela*[†]

*Physics Dept., University of California
Santa Barbara, CA, 93105, USA
E-mail: incandel@fnal.gov*

ABSTRACT: In this note I report the status and prospects of the CDF and D0 experiments in Run 2 of the Tevatron Collider at Fermilab as of March 2003. Some of the more exciting physics goals of the high transverse energy (E_T) program are reviewed. Select elements of the upgraded accelerator complex and the upgraded detectors and their performance are presented. Preliminary Run 2 results are then presented, starting with W and Z physics, and followed by top quark studies. I also include some low E_T charm and bottom physics results since bottom and charm are important ingredients in many new physics searches at high E_T .

*Dedicated to my father, Joseph R. Incandela
May 28, 1926 - May 4, 2003*

The Run 2 physics program at the Fermilab Tevatron Collider required very substantial upgrades of the CDF and D0 detectors. These upgrades will provide substantial improvement in physics capabilities. However, virtually all subsystems are far more complicated than they were in Run 1. As one example, the CDF silicon system has gone from 46,000 readout channels in Run 1 to 722,000 readout channels in Run 2. In addition, a major upgrade of the Tevatron has reduced the time between beam collisions from 3.5 μs to 396 ns which has necessitated a major change in all front end readout electronics, triggers, and data acquisition systems. Such a significant enhancement in complexity of all systems naturally carries with it major new challenges in the construction and commissioning of the detectors - both of which took longer than originally anticipated. The detectors are now becoming very well understood. While it appears that some subsystems will not meet full expectations, a significant number of detector elements are beginning to meet and exceed design goals.

*Speaker.

[†]Supported by United States Department of Energy grant number DE-FG03-91ER40618.

A continuing effort to improve the performance of the Tevatron has been underway since 2001 and has begun to show slow but steady progress in achieving higher luminosities. New all-time luminosity records have recently been attained. At the time of this writing, the data accumulated by each of the collider experiments in Run 2 is still somewhat below the total collected in Run 1. Nevertheless, many Run 1 measurements have been repeated with the new data and show comparable resolution. The substantial increases in acceptance and the new capabilities of the detectors for Run 2 have made it possible to do completely new measurements and in some cases to achieve greater resolution with less data for some repeat measurements.

In this note I will present a selection of the high E_T goals of the Tevatron collider program with references to Run 1 results and up-to-date Run 2 projections. Some of the more recent additions to the program coming from relatively new ideas in theoretical physics will also be discussed. I will then turn to the accelerator and the CDF and D0 collider detectors. I will review salient features of the upgrades and then present their current performance. Finally, based upon performance to date and current expectations for future performance, I will close this note with a very brief speculative discussion of the implications for high E_T physics in the pre-LHC era.

1. Goals of the Tevatron Collider Program

The Tevatron Collider program has a large number of physics goals. I will review a selected subset related to higher mass states that are only accessible at the energy frontier.

1.1 Standard Model Higgs

Though not an easy quarry, the Tevatron community has spent a significant amount of effort and preparation to mount a search for the Higgs boson. Within the Standard Model (SM) the combination of all precision electroweak data and direct searches [1] constrain the SM Higgs (H) to be in the low mass range $114 \lesssim M_H \lesssim 200$ GeV. ¹ In this mass range the significant decay modes of the Higgs are $H \rightarrow b\bar{b}$ and $H \rightarrow W^+W^-$ with the former dominant below $M_H = 135$ GeV and the latter dominant above this mass, as seen in figure 1. At the Tevatron, as will be true at the LHC, the dominant Higgs production mode is $gg \rightarrow H$. Unfortunately this means that for $M_H < 135$ GeV the majority of Higgs events will be indistinguishable from standard model $b\bar{b}$ production which, even at such high invariant masses, have rates many orders of magnitude above the Higgs rate. For the higher mass Higgs, W pair production has relatively low SM backgrounds and studies [3] have indicated that it can contribute meaningfully to a search provided there are adequate data, as discussed below.

For all masses, a somewhat more promising avenue is afforded by the process in which the Higgs is produced in association with an intermediate vector boson ($V = W^\pm$ or Z). Although the production rate is reduced by an order of magnitude relative to solo Higgs

¹This prediction is not free of caveats. There are two slightly anomalous contributions to the limit which would cause the expected range to fluctuate either much higher or much lower should they be removed from the global fit [2].

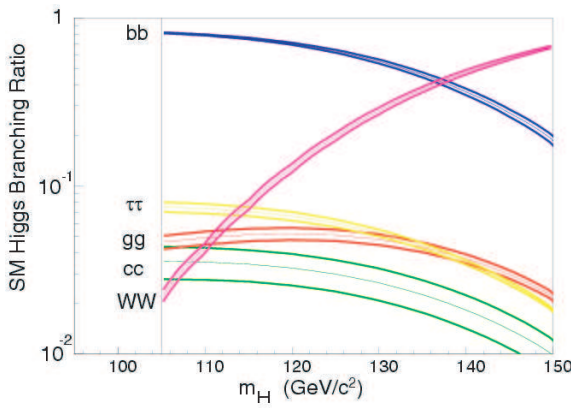


Figure 1: Branching ratios for SM Higgs decays versus mass in the range $100 < M_H < 150$ GeV.

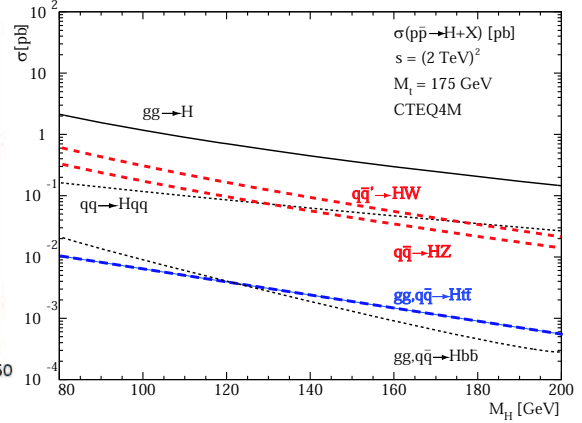


Figure 2: Production cross sections [pb] for SM Higgs alone or in association with other particles in the range $80 < M_H < 200$ GeV.

production, as seen in figure 2, these events do have a subset of final states with very distinct signatures. Particularly in those cases where the associated V decays to μ or e leptons (e.g. $W \rightarrow e\nu$, $\mu\nu$ and $Z \rightarrow ee, \mu\mu$) the presence of two high E_T leptons or one such lepton and significant missing E_T provides a strong means for rejecting SM background events.

In the range $M_H \lesssim 135$, the main backgrounds to the signatures tabulated here are those coming from $W+b\bar{b}$ and $W+c\bar{c}$ production.² While these are relatively rare events, particularly for high $b\bar{b}$ invariant pair mass, they are unfortunately still somewhat less rare than WH events. Table 1 summarizes the main backgrounds to the various signal channels.

Mass Range	Signal	Backgrounds
$M_H \lesssim 135$ GeV	$WH \rightarrow qq'b\bar{b}$	multijet production
" "	$WH \rightarrow l\nu b\bar{b}$	$Wb\bar{b}, WZ, t\bar{t}, t\bar{b}$
" "	$ZH \rightarrow l^+l^-b\bar{b}$	$Zb\bar{b}, ZZ, t\bar{t}$
" "	$ZH \rightarrow \nu\bar{\nu}b\bar{b}$	QCD $Zb\bar{b}, ZZ, t\bar{t}$
$M_H \gtrsim 135$ GeV	$H \rightarrow WW \rightarrow l^+l^-\nu\bar{\nu}$	WW, WZ
" "	$HW \rightarrow WWW$	$t\bar{t}, t\bar{t} + W$ or Z, WW or $W/Z + jets...$
" "	$HZ \rightarrow WWZ$	$t\bar{t}, t\bar{t} + W$ or Z, WW or $W/Z + jets...$

Table 1: SM Higgs Search Channels and Backgrounds at the Tevatron.

For $M_H \lesssim 135$ GeV, as seen in table 1 the signatures are comprised of tagged b jets together with missing E_T , or single lepton plus missing E_T or like-flavor opposite-sign dileptons. At higher mass, the signatures are comprised of multiple leptons, possibly with missing E_T and jets. Experimentally these event signatures require good instrumental capabilities in the areas of e and μ identification and missing E_T resolution for the vector bosons, as well as good b tagging and dijet mass resolution for $b\bar{b}$ pair reconstruction. Charm and τ identification are not needed for the signal, given the rarity of SM H decays

²In Run 1, the CDF b-tag algorithm, which was used in the discovery of the top quark, was more than $\sim 50\%$ efficient for b jets over 50 GeV and 20% efficient for high energy charm jets.

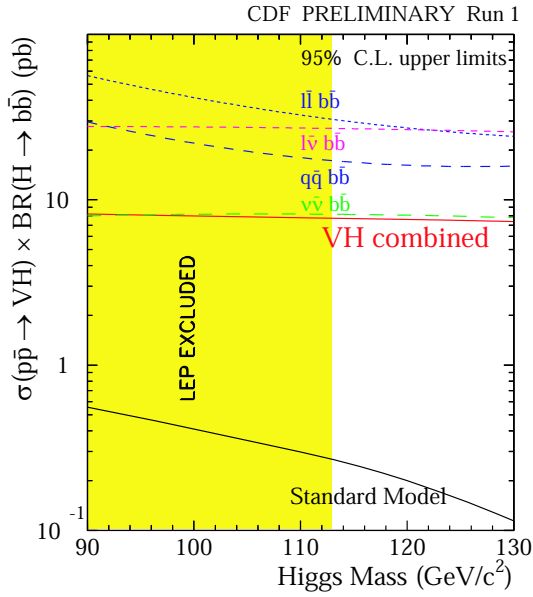


Figure 3: Limits on SM Higgs versus mass in the range $100 < M_H < 130$ GeV as determined by CDF in Run 1.

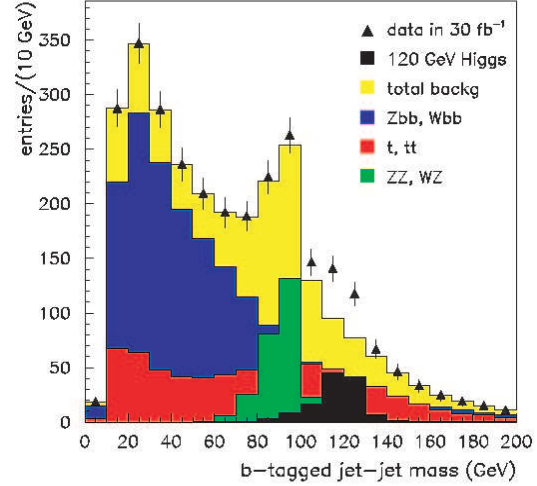


Figure 4: D0 MC study of signal and backgrounds for 120 GeV Higgs.

to these particles as shown in Figure 1. However, the capability to distinguish them from b 's would help in understanding some of the backgrounds.

In Run 1, CDF set limits on many of these channels which are 1 - 2 orders of magnitude above SM expectations as seen in Figure 3. In order to have sensitivity to SM Higgs in Run 2 we will of course need significantly more data than was available in Run 1. Even beyond the issue of integrated luminosity, a very good understanding of our backgrounds and an improved dijet mass resolution will be critical to our final sensitivity. Figure 4 shows the signal and background expectation for a 120 GeV Higgs in 30 fb^{-1} as obtained in a study by the D0 collaboration [3].

	years	bunch spacing	\sqrt{s}	Data per Expt.
Run 0	1988-89	$3.5 \mu\text{s}$	1.8 TeV	5 pb^{-1}
Run 1	1992-96	$3.5 \mu\text{s}$	1.8 TeV	120 pb^{-1}
Upgrades 1996-2001				
Run 2a	2001-2005	396 ns	1.96 TeV	$1\text{-}2 \text{ fb}^{-1}$
Upgrades 2005-2006				
Run 2b	2006-?	396 ns	1.96 TeV	$\gtrsim 6 \text{ fb}^{-1}$

Table 2: Tevatron Collider Program Timeline

With regard to the critical issue of $b\bar{b}$ dijet mass resolution a great deal of work has been done to improve upon that which was achieved in Run 1. Jet energy corrections now include corrections for the presence of muons in jets and for missing E_T [4]. Inclusion of tracking and shower maximum information as seen in Figure 5 substantially reduce

the measurement uncertainty. Monte Carlo studies now indicate a resolution of $\sim 13.5\%$ in $Z \rightarrow b\bar{b}$ events can be achieved as seen in Figure 6, representing a roughly 30 to 50% improvement over what one can obtain with calorimetry alone. CDF demonstrated already in Run 1 that a sample of $Z \rightarrow b\bar{b}$ events could be isolated as seen in figure 7. In Run 2 CDF has a new hadronic b trigger [5] that is being used to accumulate larger and more pure samples of these events which can then be used as a very important calibration for $b\bar{b}$ mass reconstruction. D0 is also in the process of preparing a displaced track trigger for high E_T events which will have similar capabilities [6].

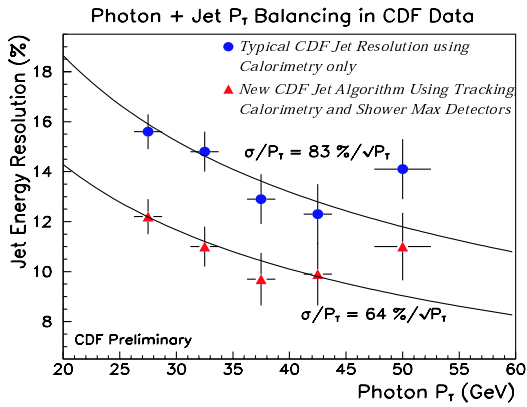


Figure 5: Jet energy resolution (%) versus photon transverse momentum in photon-jet events as measured by CDF in Run 1.

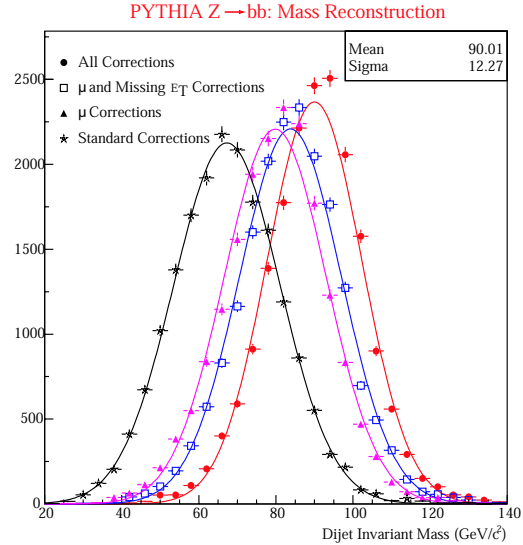


Figure 6: The invariant mass distribution for $Z \rightarrow b\bar{b}$ events in Monte Carlo is shown for various jet corrections as indicated.

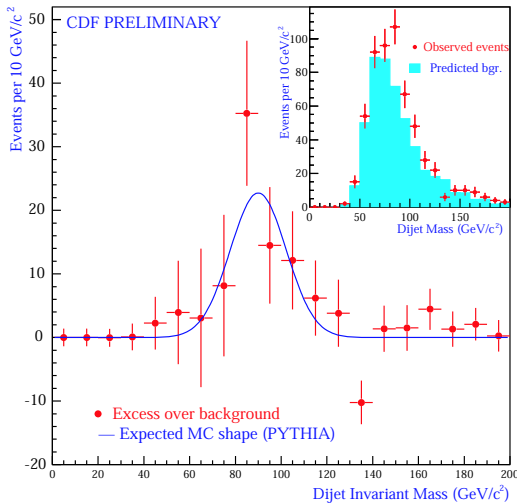


Figure 7: CDF reconstructed $Z \rightarrow b\bar{b}$ mass for events collected in Run 1.

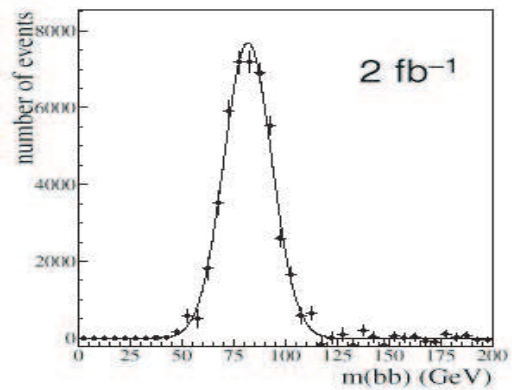


Figure 8: MC projections for $Z \rightarrow b\bar{b}$ events in 2 fb^{-1} of data collected in Run 2.

jhw2002/013

For $M_H \gtrsim 135$ GeV where the decay $H \rightarrow WW^{(*)}$ is dominant, solo Higgs production does contribute meaningfully to the signal since the backgrounds to diboson production are not quite large enough to swamp the signal completely. One must of course require leptonic (specifically e or μ) decays of the vector bosons. The backgrounds are predominantly Drell-Yan, WW , WZ , ZZ , $t\bar{t}$, single t , and $\tau\tau$ production. For the associated production of H with W or Z in this high M_H domain, there are of course spectacular trilepton signatures with missing E_T . These have very small backgrounds including many of those mentioned for solo Higgs production.

Combining all channels mentioned above for solo and associated production of SM Higgs, the potential for 95% CL exclusion or significant observation of the Higgs versus mass has been estimated [3]. The result is shown graphically in figure 9. In the making of this plot it is assumed that $H \rightarrow b\bar{b}$ decays have $b\bar{b}$ pair invariant mass resolution on the order of $\sim 10\%$ and that b tagging efficiency will be comparable to and slightly improved over that obtained by CDF in Run 1. In addition, the results are based upon optimised sensitivities obtained by means of neural nets [7]. Recent preliminary crosschecks of these results have concluded that the required luminosities could be roughly 20% higher than those indicated in figure 9. The largest increase was in relation to the invariant mass of the $b\bar{b}$ pair. As noted above, resolution on the order of 13% looks to be achievable while 10% is too optimistic [8]. More work is in progress to update the Tevatron sensitivities to SM Higgs.

A red band in the figure indicates the luminosity range where we expect the performance of the silicon detectors to become significantly compromised by radiation damage [9]. It should be clear to the reader that the discovery of a standard model Higgs at the Tevatron will not be easy. In particular it requires the accelerator to work well and produce lots of data while the experiments simultaneously operate at peak levels for many years. In addition, backgrounds must be extremely well understood, and silicon detectors may need to be rebuilt and replaced after a few fb^{-1} of data have been accumulated by each experiment. It is a rather daunting task!

One can also consider what would happen if the Higgs turned out to have a mass of ~ 115 GeV which is where some interesting events were seen by the LEP II experiments [1]. Table 3 lists expected signal and background events for 15 fb^{-1} integrated luminosity. It turns out that this mass can in fact be excluded at 95% CL

Mode	N(Signal)	N(Background)	S/\sqrt{B}
$l\nu b\bar{b}$	92	450	4.3
$l\nu b\bar{b}$	90	880	3.0
$l^+l^-b\bar{b}$	10	44	1.5

Table 3: SM Higgs signal and background events per experiment in 15 fb^{-1} for various modes with $M_H = 115$ GeV.

by the Tevatron experiments with a little more than 2 fb^{-1} of data. To observe 3 and 5 σ excesses will require 5 and 15 fb^{-1} , respectively.

The difficulty of the SM Higgs search at the Tevatron has motivated new investigations and re-evaluations of modes other than those discussed above. Two modes under investigation recently are $p\bar{p} \rightarrow Hb$ (“single b ” associated production) [10] and $p\bar{p} \rightarrow t\bar{t}H$ [11]. The cross section for single b associated production with Higgs is shown at leading order (LO) and next to leading order (NLO) in figure 10. Single b associated production is more

than an order of magnitude higher than $b\bar{b}$ associated production. In the past this channel was not seriously considered due to the difficulty of triggering on events - particularly at low Higgs mass where $H \rightarrow b\bar{b}$. With the advent of silicon track triggers for hadronic b baryon and meson decays, it is possible to overcome this problem.

The associated production of Higgs with $t\bar{t}$ was also reconsidered in recent years after the Tevatron luminosity goal was extended well beyond 2 fb^{-1} . Previously the production rate was considered too small. For low Higgs mass, if the $t\bar{t}$ portion of such an event could be reconstructed adequately to isolate the b jets from Higgs, then it turns out that the signal stands out relative to the irreducible backgrounds as seen in figure 12. The ability to simply associate all the decay products to $t\bar{t}$ correctly is quite difficult and there has been no indication that it can be done with more than about 50% efficiency. An alternative approach that escapes this difficulty is to simply find the 4 best b jet candidates and to form their 6 possible pairings. The corresponding 6 invariant masses, when plotted in descending order, yield distributions that are distinctly different from the corresponding distributions for $t\bar{t}jj$ background as seen in figure 13.

1.2 Minimal Supersymmetric Higgs (MSSM)

The MSSM extends the Standard Model Higgs sector to include 2 complex scalar SU(2) doublets [12]. The two doublets result in a spectrum of five Higgs bosons denoted h , H , A^0 , H^+ and H^- . The neutral h is the lightest of the five and can have couplings and decays similar to the SM Higgs. The H and A^0 are the CP even and odd scalar Higgs bosons whose masses are expected to be high. The charged Higgs' H^\pm are also generally expected to be massive. All of the masses can be parametrized in terms of two parameters, typically taken to be M_A and $\tan(\beta) = v_2/v_1$ where v_i is the vacuum expectation value of the i^{th}

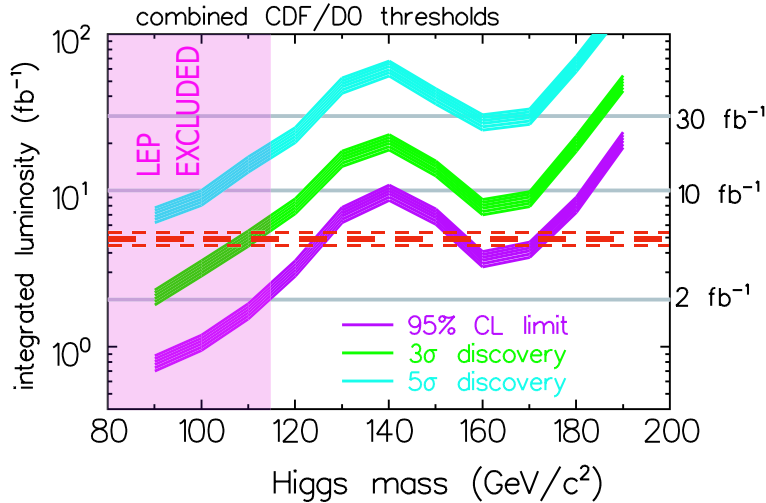


Figure 9: Three contours show the potential for the combined CDF and D0 data sets to exclude SM Higgs at 95% CL or to observe it at 3 and 5 σ significance as a function of M_H and luminosity. The red band indicates the luminosity range where it is expected that the silicon detectors may become severely damaged by radiation.

Higgs doublet [13].

At the Tevatron, the main search focus will be on the h . Rather stringent theoretical limits combined with experimental limits from LEP and from CDF in Run 1 already exist for h . These are displayed in the $\tan(\beta)$ versus M_h plane in figure 14. The production cross sections of h , H , and A^o at large $\tan\beta$ are enhanced by their couplings to b quarks via the diagrams shown in figure 15. In run 2 CDF and D0 will have the capability to exclude the MSSM with 5 fb^{-1} of data in almost all of the M_A - $\tan\beta$ plane up to $M_A \sim 400 \text{ GeV}$ as shown in figure 16. Only in the most challenging scenario in which the couplings to $b\bar{b}$ are suppressed (lower left plot) are there some small regions that are not accessible. Discovery however will require significantly more integrated luminosity.

1.3 Supersymmetric Particles

Squarks and gluinos are the most copiously produced supersymmetric (SUSY) particles at hadron colliders and have very distinct final states in some instances. The two most promising possibilities are gluino pair production with cascade to like-sign dileptons as seen in figure 17 or gauginos to tripletons as seen in figure 18. In the former case the decay chain can include 2 standard model W gauge bosons of the same sign. In the diagram shown, R parity is assumed to hold and the neutralino is assumed to be the lightest SUSY particle (LSP). The tripleton decay chain of the gauginos is also an experimentally clean search channel. Combining the dilepton and tripleton searches allows significant limits to be placed on $\sigma \cdot Br$ for gaugino pair production and decay in the SUGRA model [14] as seen in figure 19. With integrated luminosities of several fb^{-1} a significant portion of unstudied SUSY parameter space can be covered.

As a last example of the prospects for discovering supersymmetry at the Tevatron, the lightest stop \tilde{t}_1 is a very good search candidate [15]. The \tilde{t}_1 could be the lightest squark as a result of the mixing angle θ_t between the superpartners of the left- and right-handed top quarks, namely \tilde{t}_L and \tilde{t}_R . These form the lightest stop mass eigenstate:

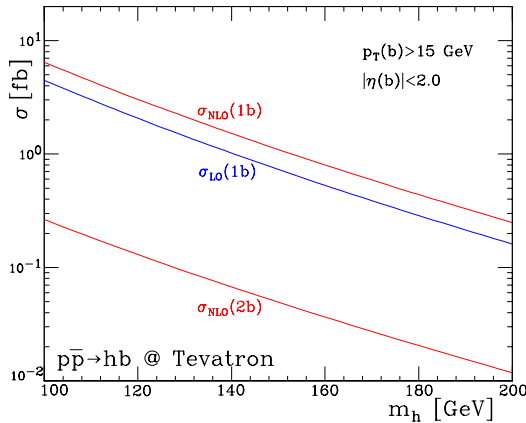


Figure 10: Associated production of a single b with SM Higgs at LO and NLO compared to associated production of $b\bar{b}$ with SM Higgs.

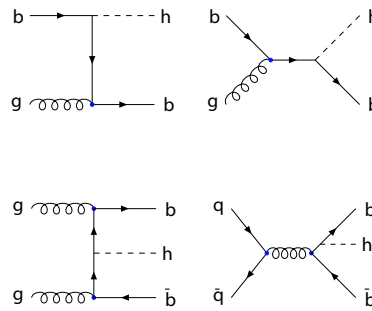


Figure 11: Representative Feynman diagrams for production of higgs in association with a single b (top) and $b\bar{b}$ (bottom).

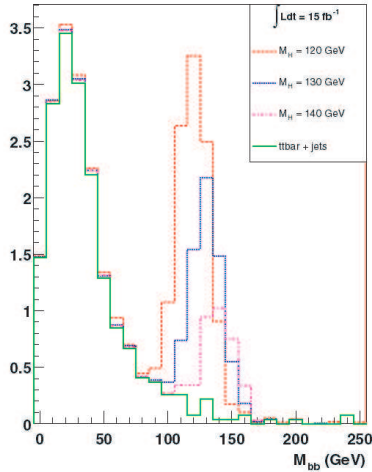


Figure 12: Monte Carlo study showing the invariant mass of the “extra” $b\bar{b}$ pair in $t\bar{t}H$ events compared to the irreducible background from $t\bar{t}g$. The plots are for the unrealistic case in which all the objects that come from the $t\bar{t}$ decay are properly associated to $t\bar{t}$ so that the extra $b\bar{b}$ is correctly isolated.

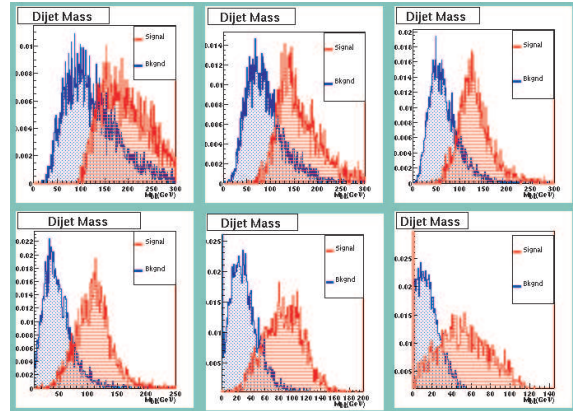


Figure 13: The 6 candidate $b\bar{b}$ pair mass distributions in $t\bar{t}H$ (red) and $t\bar{t}g$ (blue) with $g, H \rightarrow b\bar{b}$. The pair masses are ordered in each event from highest to lowest values, providing a strong distinction between signal and background.

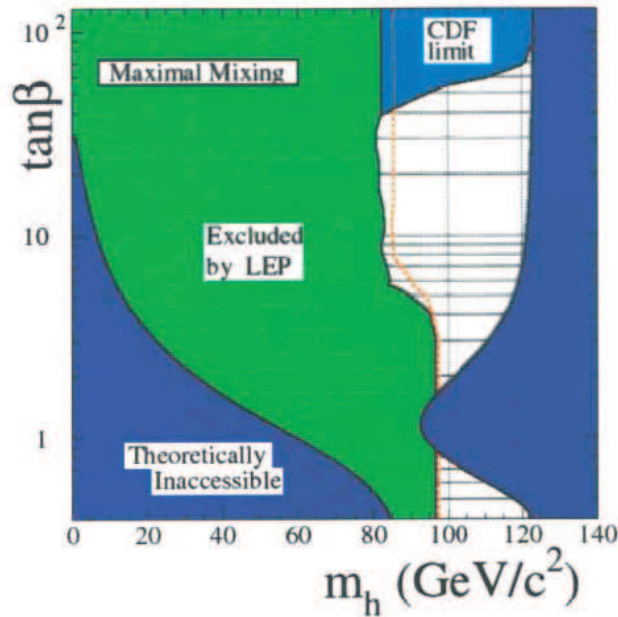


Figure 14: Theoretical and experimental limits on the lightest MSSM Higgs.

$\tilde{t}_1 = \tilde{t}_L \cos\theta_t + \tilde{t}_R \sin\theta_t$. Alternatively one could argue that the mass should be low relative to other squarks as a result of the fact that the top has the largest known Yukawa

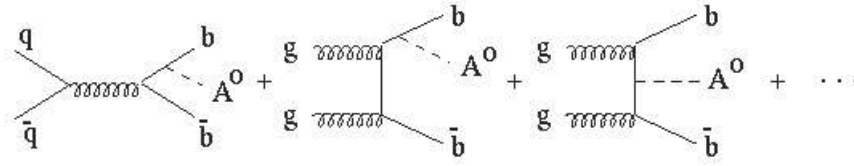


Figure 15: Production mechanisms for the CP-Odd MSSM Higgs A^0 in association with $b\bar{b}$.

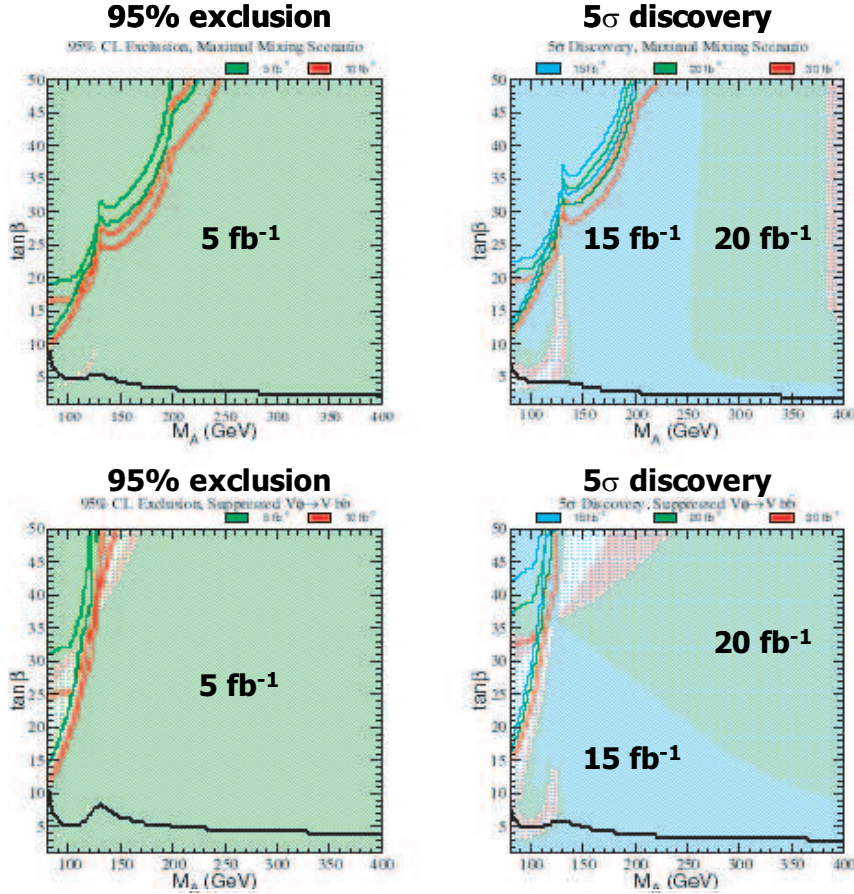


Figure 16: Run 2 projections for the potential to discover or exclude the lightest MSSM Higgs in the $\tan\beta$ versus M_A plane.

coupling ($\Lambda_t \approx 1$). In any case, with a few fb^{-1} of data, \tilde{t}_1 could be excluded (discovered) up to masses of 200 (160) GeV via top-like decays $\tilde{t} \rightarrow \tilde{\chi}^\pm \rightarrow b\tilde{\nu}$ or final states containing charm: $\tilde{t} \rightarrow \tilde{\chi}^\pm b \rightarrow b\tilde{\chi}^0 c$. In both cases, since the dominant production mode is $t\bar{t}$ pair production, the final states are very distinct. In the former case, it's very similar to the $t\bar{t}$ final state, possibly at a different mass scale, while in the latter case one would look for evidence of $c\bar{c}$ and large missing E_T .

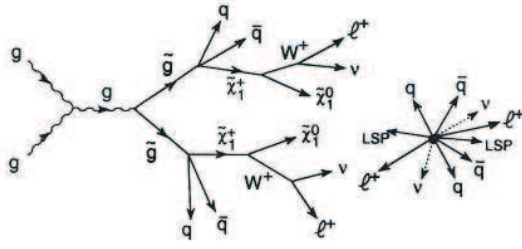


Figure 17: A distinctive and background free decay sequence for massive gluinos with like-sign dileptons in the final state.

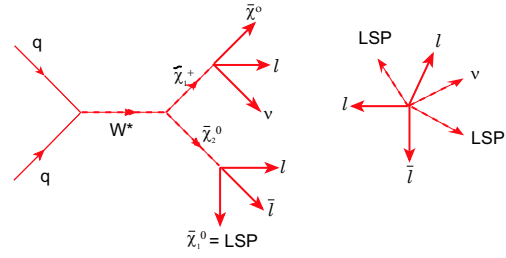


Figure 18: The tripletonic decay of gaugino pairs is also an extremely clean channel.

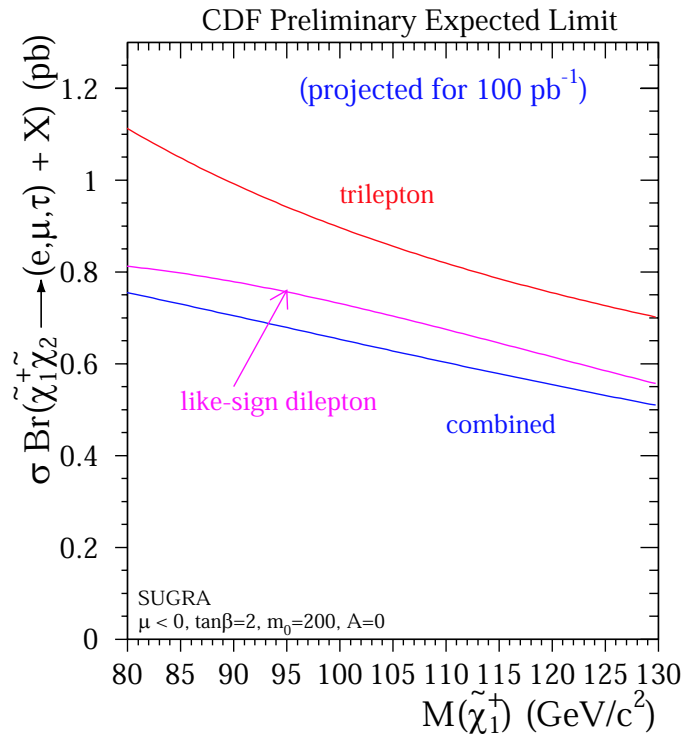


Figure 19: Average expected limit on $\sigma \cdot Br$ as a function of the mass of $\tilde{\chi}_1^\pm$ for like-sign dilepton and tripleton searches and their combination, per 100 pb^{-1} of data collected.

2. The Search for Large Extra Dimensions (LED)

While there are currently no known direct tests of modern string theories, circumstantial evidence for these theories would be afforded by any experimental indication of the existence of additional large dimensions beyond the 3+1 ordinary dimensions of everyday life. Several new phenomenological models of LED have arisen in recent years with potentially observable consequences. One of the earliest and perhaps most intuitively simple, is that of Arkani-Hamed, Dimopolous and Dvali (ADD) [16]. Other models such as that of Randall and Sundstrum [17] have a similar basis but different phenomenology. In these models large

extra dimensions are used to explain the enormous difference between our low energy world and the Planck scale by positing that the weakness of gravity is only an apparent weakness due to the fact that the majority of the gravitational field's flux of Kaluza-Klein gravitons (G_{KK}) propagate into extra dimensions. A Gauss surface in a space that includes the δ additional dimensions then provides the fundamental mass scale M_D which can be many orders of magnitude smaller than the Planck scale. In the ADD model, Newton's constant G_N can be related to the number δ of LEDs, their size R , and M_D , via the expression:

$$G_N^{-1} = 8\pi R^\delta M_D^{2+\delta}$$

The coupling of the graviton to SM particles is extremely weak but large R means there's significant phase space. The G_{KK} states form a continuum. At collider energies the couplings are on the order of $(E/M_D)^{2+\delta} \sim 1$ where E is the process energy and one assumes that $M_D \sim 1$ TeV. For M_D at this scale, deviations from Newton's law are expected at distances on the order of $R \lesssim 10^{(32/\delta-19)}$. Current direct gravitational measurements see no deviations down to scales on the order of 100 - 200 μm [18, 19]. This would eliminate $\delta \leq 2$.

Several searches for LEDs have been performed at the Tevatron in Run 1 and will be extended in Run 2. D0 performed a search for direct production of G_{KK} with subsequent decay to e^+e^- or $\gamma\gamma$. For $\delta = 2$ they set a limit on M_D of 1.4 TeV. [20] In Run 1b CDF searched for LEDs in a sample of events containing single γ and large missing E_T [21]. After all selections, there remained 11 candidates in 87 pb^{-1} of data as seen in figure 20. Limits on M_D of 549, 581 and 602 GeV were set for $\delta = 4, 6$ and 8. In Run 2 it will be possible to extend these limits above ~ 1 Tev with a few fb^{-1} of data [22].

2.1 Electroweak Studies

While hadron collider experiments are generally regarded as excellent discovery vehicles, it is not always appreciated just how well they can perform high precision measurements - comparable to lepton colliders in many cases. [23] The CDF and D0 measurements of the W mass are good examples. The combined Run 1 result for the Tevatron is [24]:

$$M_W = 80.456 \pm 0.059 \text{ GeV}$$

When combined with the preliminary LEP results, this yields a world average of

$$M_W = 80.450 \pm 0.034 \text{ GeV}$$

The precise measurement of M_W is particularly important when taken in combination with a precise measurement of the mass of the t quark. Radiative corrections to the W

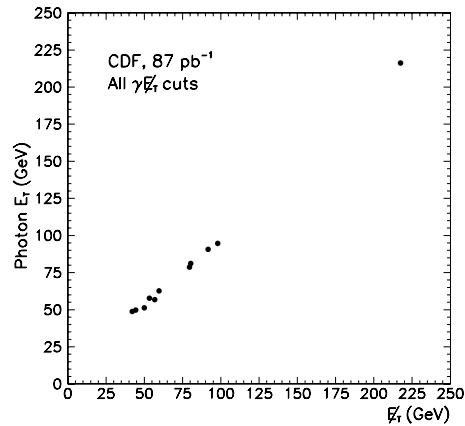


Figure 20: Photon E_T versus missing E_T for the 11 events surviving all selections in the CDF Run 1 search for LED.

self energy depend quadratically on the top mass and logarithmically on the SM Higgs mass. The precision measurement of M_W and M_t thus allows one to constrain the mass of the Higgs as represented by the larger circle in the M_W versus M_t plane shown in figure 21. Run 1 results, combined with LEP and other electroweak measurements currently constrain M_H to be relatively small, as discussed above, but with large uncertainty. With 2 fb^{-1} the Tevatron experiments are expected to reduce the errors on M_W and M_t to 30 MeV and 3 GeV per experiment, respectively. This will constrain the SM Higgs mass to the smaller circular contour³ shown in figure 21 [25]. The expected improvements are mainly due to the increase in integrated luminosity but a variety of system upgrades also contribute substantially to this projection. The increase in center of mass energy to $\sqrt{s} = 1.96 \text{ TeV}$ in Run 2 from 1.8 TeV in Run 1 increases the production cross-sections for W and Z by $\sim 10\%$ and for top by $\sim 35\%$. Detector upgrades increase acceptance for b jet and lepton identification and triggering. The detectors are on track to meet these expectations.

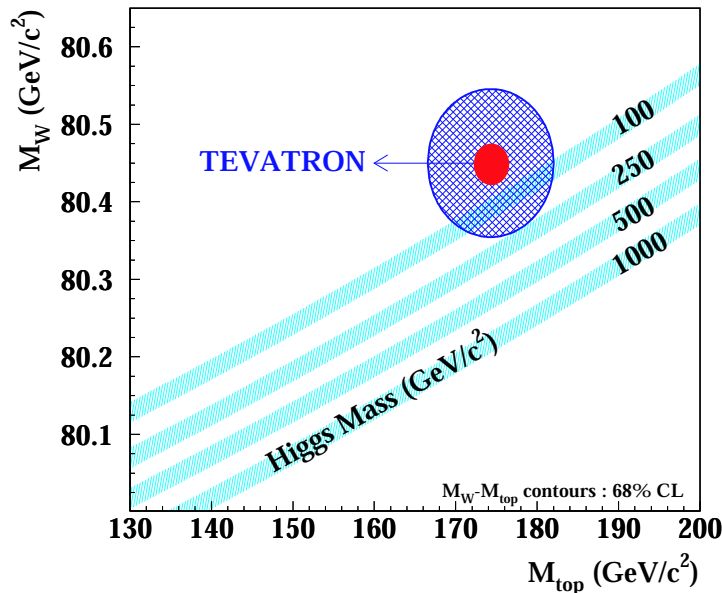


Figure 21: Standard Model Higgs mass constraint contours in the M_W versus M_{top} plane in Run 1 (blue) and projected for 2 fb^{-1} of data in Run 2a (red).

3. Status of the Tevatron, CDF and D0

3.1 The Fermilab Collider

The Fermilab Tevatron accelerator complex, shown in figure 22, has undergone extensive upgrades [26]. The most significant of the upgrade projects is the construction of the new Main Injector which replaces the old Main Ring as an intermediate energy accelerator prior

³This is only an approximate projection in which I have assumed that the CDF and D0 results can be added in quadrature. Also, the centerpoint of the red Run 2 contour is taken to be the same as that of the blue contour which need not be the case.

to injection of beams into the Tevatron [27]. The Main Injector is more reliable and can handle higher beam currents than was possible in the old Main Ring. This ultimately leads to higher luminosity in the Tevatron. Another important aspect of the luminosity upgrade is the bunch structure of the Tevatron itself. It has been increased from 6 proton on 6 anti-proton bunches with a bunch crossing time of $3.5 \mu s$ to 36 on 36 and a crossing time of $396 ns$. This allows the higher luminosity to be spread in such a manner that it does not lead to significant event pile-up in the collider experiments as a result of multiple $p\bar{p}$ collisions per bunch crossing. As in Run 1, for which the peak instantaneous luminosity was on the order of $1.5 \times 10^{31} cm^{-2} s^{-1}$, the number of multiple collisions per crossing will typically be in the range of 1 to 3. In run 2 the peak luminosity is expected to be an order of magnitude or more greater, but the additional bunches will allow the typical number of multiple interactions to remain in the same range.

In addition to the Main Injector, there is an additional storage ring in the same tunnel. The Recycler is an 8 GeV storage ring intended to increase the \bar{p} supply for the Tevatron collider by efficiently stacking bunches from the Accumulator ring and cooling them stochastically. An electron cooling system is also under development and could significantly enhance the Recycler performance.

The luminosity performance of the Tevatron has been somewhat below expectations but nevertheless has shown steady increases as seen in figures 23 and 24 [29]. Record luminosities have been regularly achieved in the past year. Overall Run 2a and Run 2b goals are presented in table 4.

Run 2a Goal $\sim 2 \text{ fb}^{-1}$ by 2005	
Peak Luminosity	Configuration
$5-8 \times 10^{31} \text{ cm}^{-2} s^{-1}$	without recycler
$1-2 \times 10^{32} \text{ cm}^{-2} s^{-1}$	with recycler
Run 2b Goal $\sim 7-10 \text{ fb}^{-1}$ before LHC	
$4-5 \times 10^{32} \text{ cm}^{-2} s^{-1}$	electron cooling

Table 4: Tevatron Run 2 goals.

3.2 The D0 Experiment

The D0 experiment as seen in figure 25 has undergone a very extensive set of upgrades for Run 2 [30]. The main upgrades are schematically represented in figures 26 and 27. An all new central tracking detector has been built and installed inside of a new 2 Tesla solenoidal magnet. The new high resolution tracker includes a silicon strip detector made up of both barrels and disks and a novel fiber tracker at larger radii. A schematic diagram of the silicon is seen in figure 28. The barrels contain 4 layers of single and double-sided silicon strips spanning the radial space from 2.7 to 9.4 cm. The double-sided barrel silicon has stereo angles of 2 and 90 degrees [31]. Small disks are interleaved with the barrels while larger ones are stationed in the far forward regions. The disks allow forward tracking to $|\eta| \sim 3$. The general characteristics of the D0 silicon are listed in table 5. The performance of the silicon is exemplified by the mass resolution seen in the silicon-only reconstruction of $K_S \rightarrow \pi^+ \pi^-$ and $\Lambda \rightarrow p \pi^-$ shown in figure 29. The functionality of the D0 silicon exceeds $\sim 95\%$ with efficiency of $\sim 97\%$. A level 2 silicon track trigger is also under construction [32].

The D0 fiber tracker [33] is shown in figure 30. The fiber tracker uses Visible Light Photon Counters (VLPC) to detect the light in the fibers generated by ionizing particles.

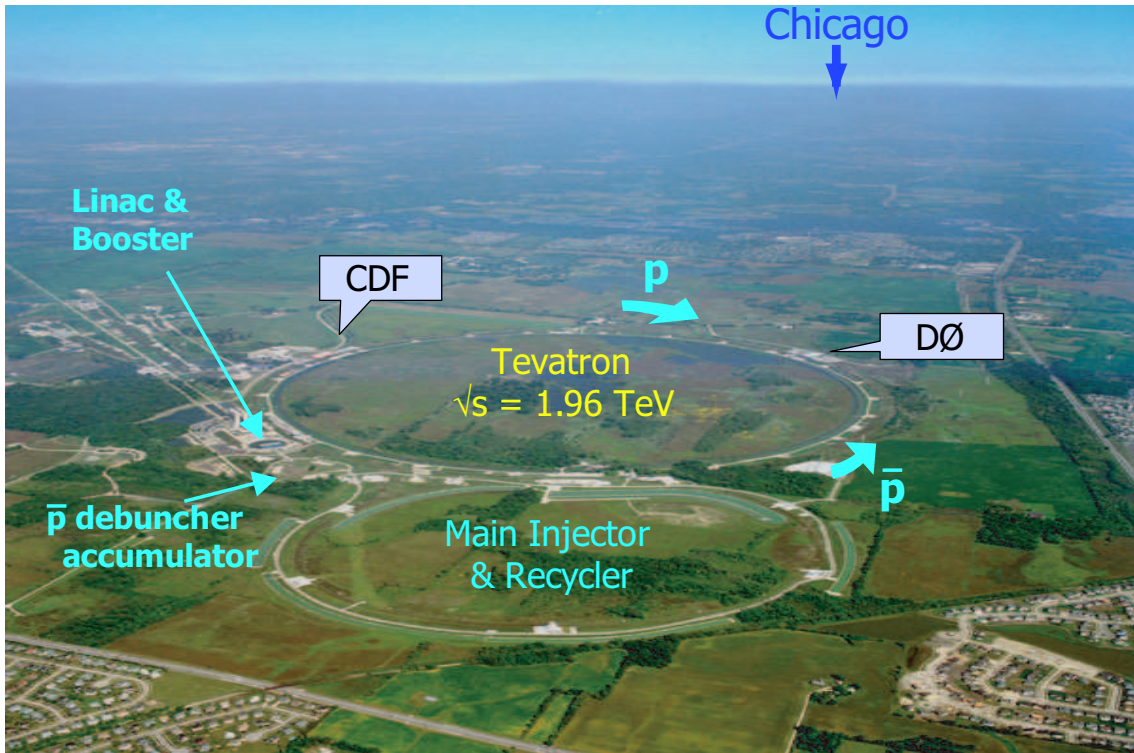


Figure 22: Fermilab Accelerator complex.

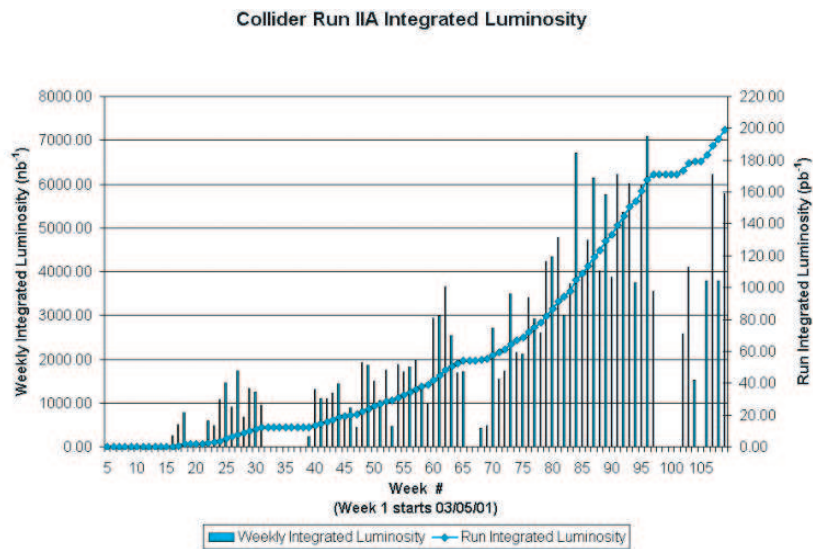


Figure 23: Integrated luminosity versus time in Run 2 of the FNAL Tevatron.

The VLPC operate at roughly 10^0 K and have quantum efficiencies on the order of 90% resulting in negligible hit inefficiencies. As can be seen in figure 31 the mass resolution is significantly increased with the addition of the larger lever arm and subsequent momentum

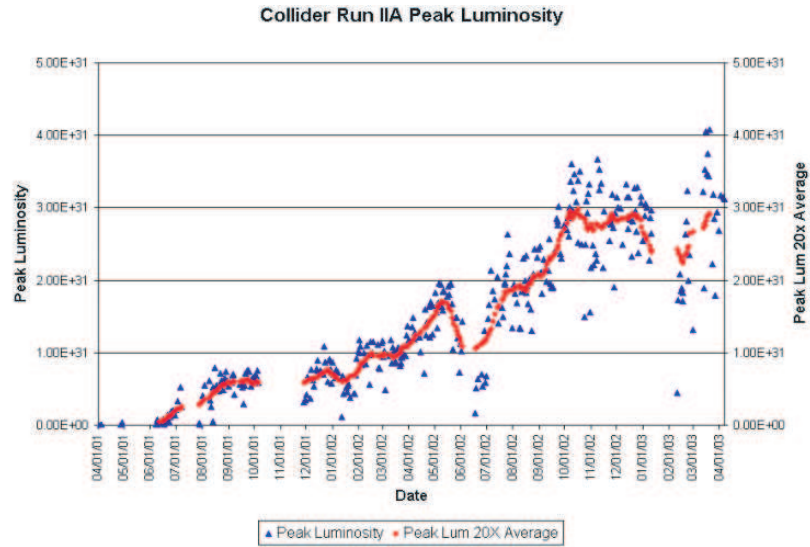


Figure 24: Peak luminosity versus time in Run 2 of the FNAL Tevatron.

resolution improvements of the fiber tracker.

The D0 tracker obtains silicon-only impact parameter resolution $\sigma_d \approx 95 \mu\text{m}$ for tracks with $p_T = 3 \text{ GeV}$. This improves to $\sigma_d \approx 37 \mu\text{m}$ when the silicon is combined with the



Figure 25: Photograph of the D0 experiment for Run 2.

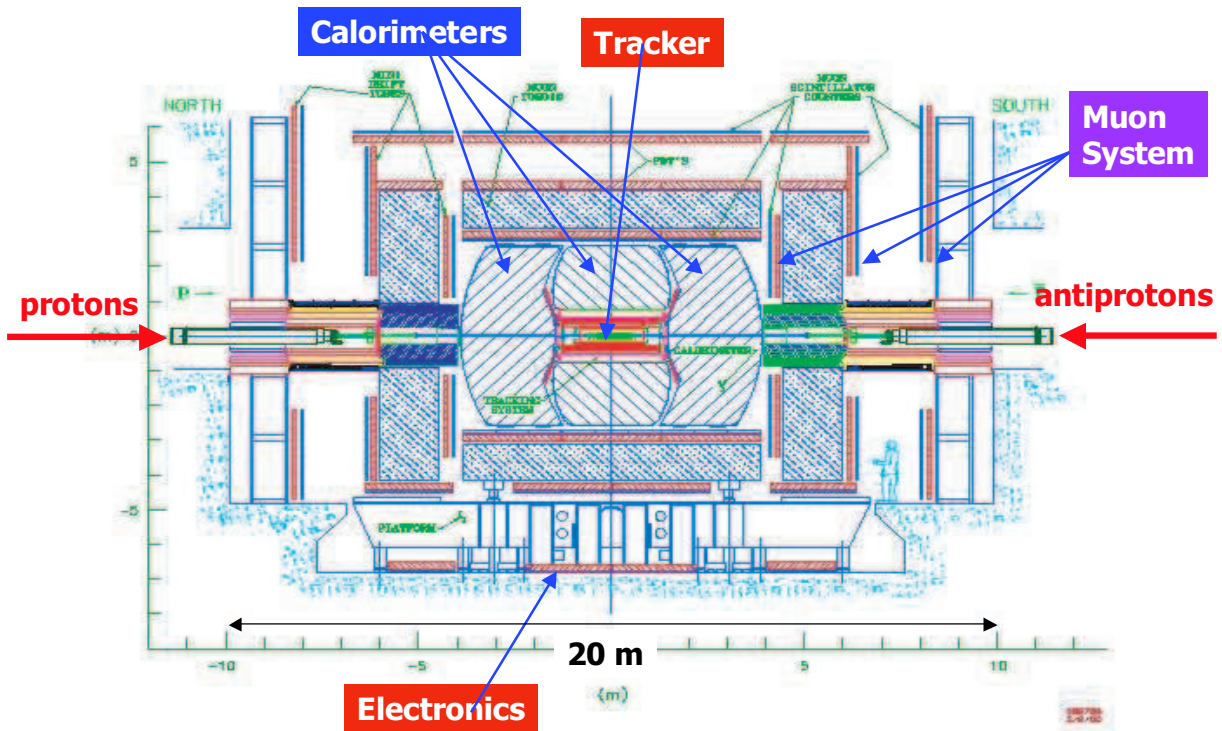


Figure 26: Schematic drawing of the D0 experiment for Run 2.

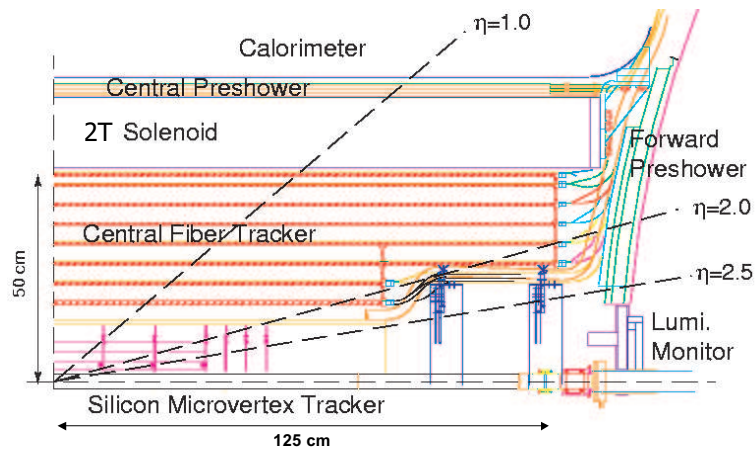


Figure 27: Schematic drawing of one quadrant of the new D0 central tracking region.

fiber tracker. With the full tracker, the momentum resolution is $\sim 2\%$ at $p_T = 1 \text{ GeV}$ for $|\eta| < 1$.

In addition to the central detector and solenoid upgrades of D0, the detector electronics, triggers and data acquisition have all been substantially upgraded to deal with the dramatically reduced bunch crossing time in Run 2 [34].

	Barrels	Small disks (F)	Large Disks (H)
Silicon	1- and 2-sided	2-sided	1-sided
Pitch angles	0, 2, 90°	±15	±7.5
Channels	387,072	258,048	147,456
Modules	432	144	96
Inner radius	2.7 cm	2.6	9.5
Outer radius	9.4 cm	10.5	26

Table 5: D0 silicon.

3.3 The CDF Experiment

The CDF experiment has also undergone extensive upgrades and changes in preparation for Run 2 [35]. The Run 2 detector during roll-in for Run 2 commissioning is shown in figure 32. The systems which have been fully or partially upgraded are indicated in figure 33. The only parts of the detector that were left unchanged are the central calorimeter and solenoid. The front-end electronics for all detector subsystems, including the central calorimeter, were upgraded to handle the shorter Tevatron bunch crossing time in Run 2. The muon system was partially upgraded to complete the coverage in the central region ($|\eta| < 1$). As was true for D0, the most extensive detector upgrades were in the tracking region. The entire CDF tracking system was rebuilt for Run 2 with the exception of the 1.4 T solenoid which was retained from Run 1.

The largest new tracking component is the Central Outer Tracker (COT) [36] which replaced the Run 1 Central Tracking Chamber (CTC) [37]. Like the CTC the new COT is a wire drift chamber. Tracks passing radially through the COT encounter 96 wireplanes which are organized into 8 superlayers. The superlayers alternate between axial and 3° stereo angle. Within a superlayer wires are organized in cells of 12 sense wires, intermixed with potential wires. The cells are tilted 35° to compensate for the Lorentz angle. Each cell of 12 wires is enclosed by cathode field sheets. This creates a uniform and isolated 0.88 cm drift region. By comparison, the CTC wires were not grouped into isolated cells. The isolated cell structure enables higher luminosity operation by limiting occupancy. Fast gas is also used to speed the collection time and to limit pile-up.

The COT performance met expectations very early in Run 2. Figure 34 shows the single hit resolution of the COT “right out of the box”, (i.e. with only very preliminary

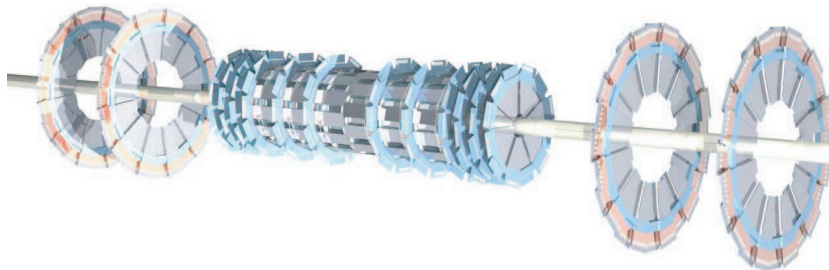


Figure 28: Solid model drawing of the D0 silicon for Run 2a.

alignment and calibration) as measured with electrons from $W \rightarrow e\nu$ decays. The single hit resolution is $175 \mu\text{m}$ which is slightly better than the design goal of $180 \mu\text{m}$. The track efficiency in these events is measured to be $\epsilon = 99 \pm 1\%$. The first measurements of momentum resolution indicate $\sigma(P_T)/P_T^2 \lesssim 0.13\% \text{ GeV}^{-1}$ as compared with a final Run 1 resolution of $0.10\% \text{ GeV}^{-1}$. Residual misalignments in the COT are factors of 2-3 smaller than they were in Run 1 due to improved bulkheads and construction techniques. At lower energy, a profile histogram of the J/ψ mass as measured with $J/\psi \rightarrow \mu^+\mu^-$ versus the difference in the cotangent of the pitch angle of the track helices is shown in figure 35. One sees that the mass varies less than 1 MeV.

The COT is used in every level of the CDF trigger. The level 1 track trigger is the eXtremely Fast Tracker (XFT) [38]. The XFT is fed the output of the COT Time-to-digital converters (TDC) and sorts hits into “prompt” (drift time $\lesssim 44\text{ns}$) or “delayed” (longer drift times). These bits are set within 132 ns of hit arrival and transmitted to hit finder boards which have dictionaries of prompt and delayed hits corresponding to segments of valid tracks contained in a total of 336 Field Programmable Gate Arrays (FPGA). When a segment mask is matched, the ϕ and slope of the segment are retained for use in a “Linker” system. The Linker compares all found segments to another dictionary of masks representing valid track candidates. There are a total of 288 FPGA’s which each cover a 1.25° slice in ϕ . The number of valid roads varies inversely with the threshold in p_T for the tracks considered. For a 1.5 GeV threshold, there are 2400 roads. Figure 36 is a single event display showing the close proximity of an online XFT track to the final reconstructed offline track. The track trigger efficiency is shown in figure 37. The efficiency is $> 95\%$ for $p_T \geq 1.5 \text{ GeV}$. The design specifications and actual resolutions are provided in table 6.

Moving radially outward from the COT is the Time of Flight (TOF) detector [39]. This system is comprised of scintillator bars lining the inner bore of the solenoid as seen in figure 38. The early performance for p , K , and π sep-

Quantity	Design	Actual
$\sigma(p_T)/P_T^2$	$1.8\% \text{ GeV}^{-1}$	$1.8\% \text{ GeV}^{-1}$
$\Delta\phi$	$< 8 \text{ mrad}$	6 mrad

Table 6: XFT Resolution.

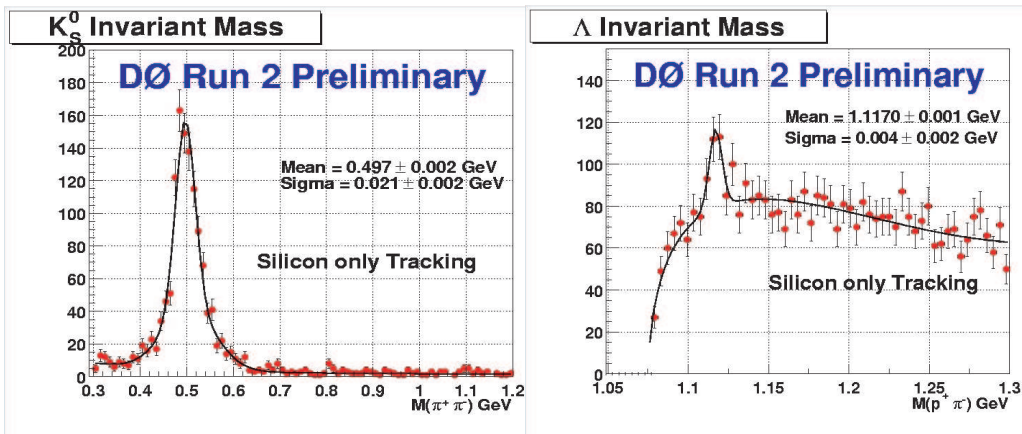


Figure 29: The reconstruction of K_s and Λ in D0 using silicon-only tracks.

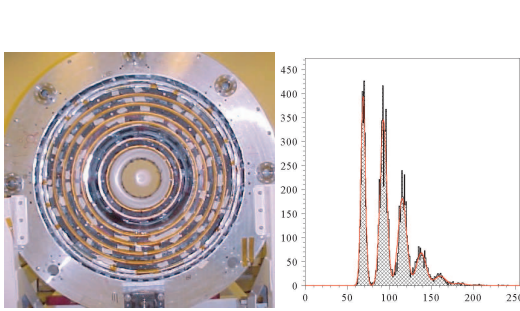


Figure 30: End view of the D0 fiber tracker. The high quantum efficiency of the VLPC's enable individual photons to be resolved and counted as shown here.

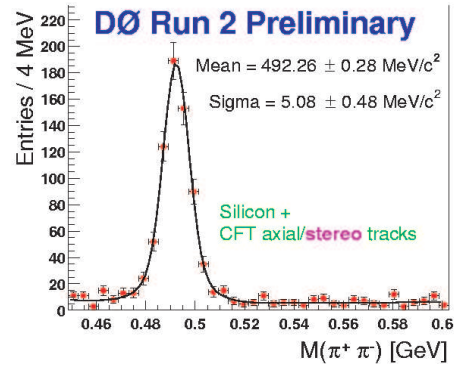


Figure 31: Performance of the complete D0 tracker as exemplified in reconstruction of $K_s \rightarrow \pi^+ \pi^-$.

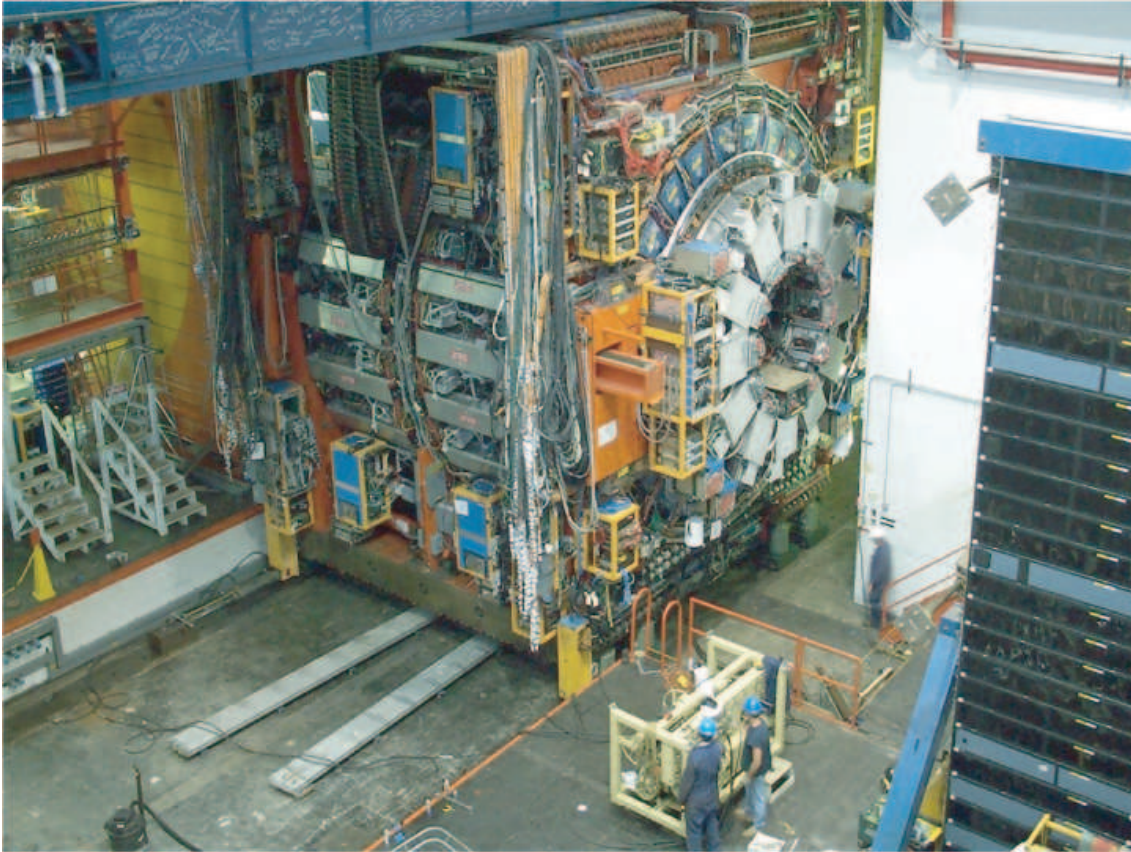


Figure 32: The CDF detector rolling into the collision hall for the Run 2 commissioning phase.

ation at low momenta is represented in figure 39. The timing resolution of the TOF is determined to be roughly 120-130 ps, falling a bit short of the design goal 100 ps. It is however expected that with improved calibrations and algorithms the design resolution

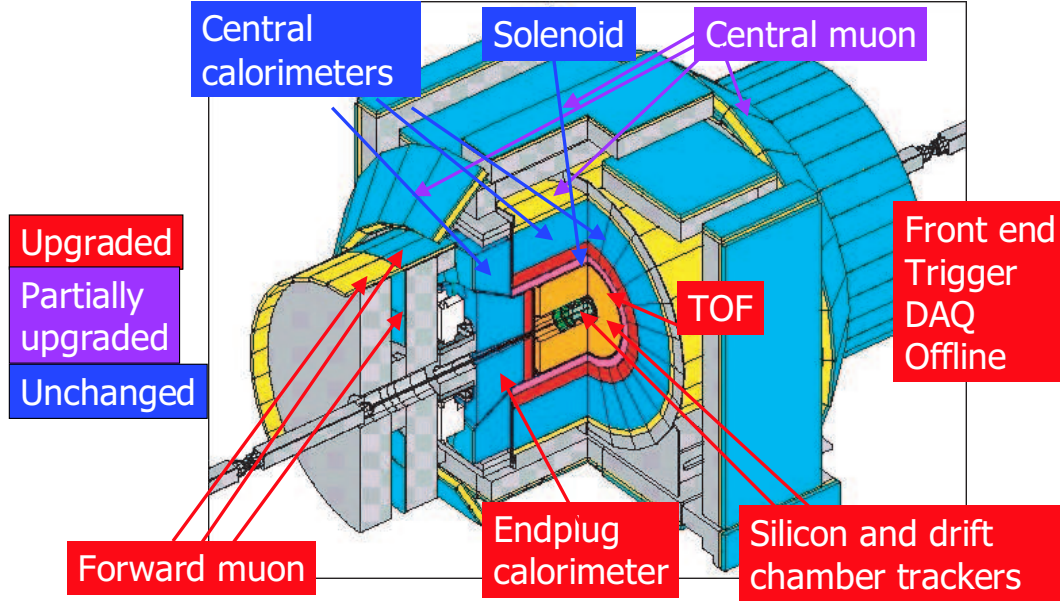


Figure 33: Isometric drawing of the CDF upgrades indicating those subsystems that have been fully or partially upgraded, or left unchanged.

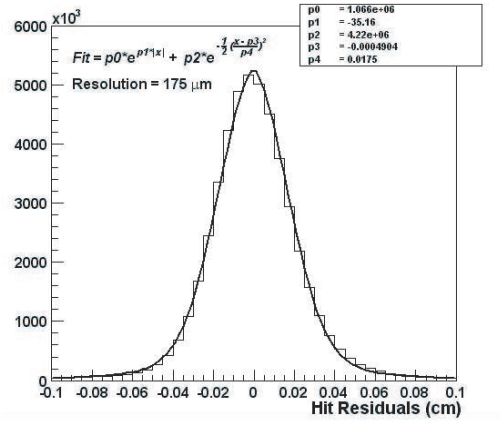


Figure 34: Electron tracks from $W \rightarrow e\nu$ events are used to determine the COT resolution at the start of operation.

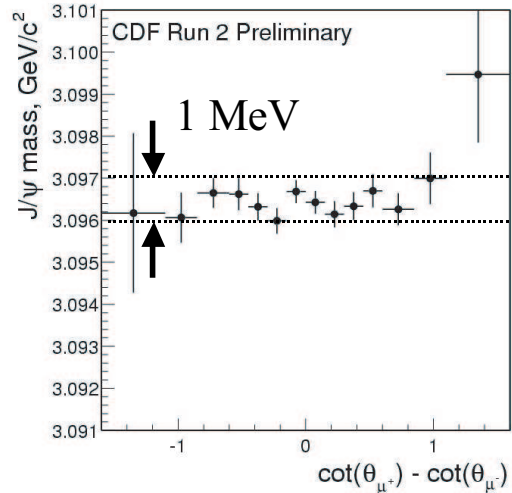


Figure 35: The uncertainty on the reconstructed J/ψ mass in $J/\psi \rightarrow \mu^+\mu^-$ as a function of the difference in the cotangent of the pitch angle of the track helix.

will be approached in the future.

The TOF detector will be used extensively for low energy phenomena, particularly in the realm of b , and c physics. The impact of the TOF for low mass spectroscopy is demonstrated clearly in the reconstruction of $\phi \rightarrow K^+K^-$ in figures 40 and 41.

Recently the TOF has been used to search for charged massive stable particles. As an example, the stop quark \tilde{t} could be stable if it were the lightest supersymmetric particle

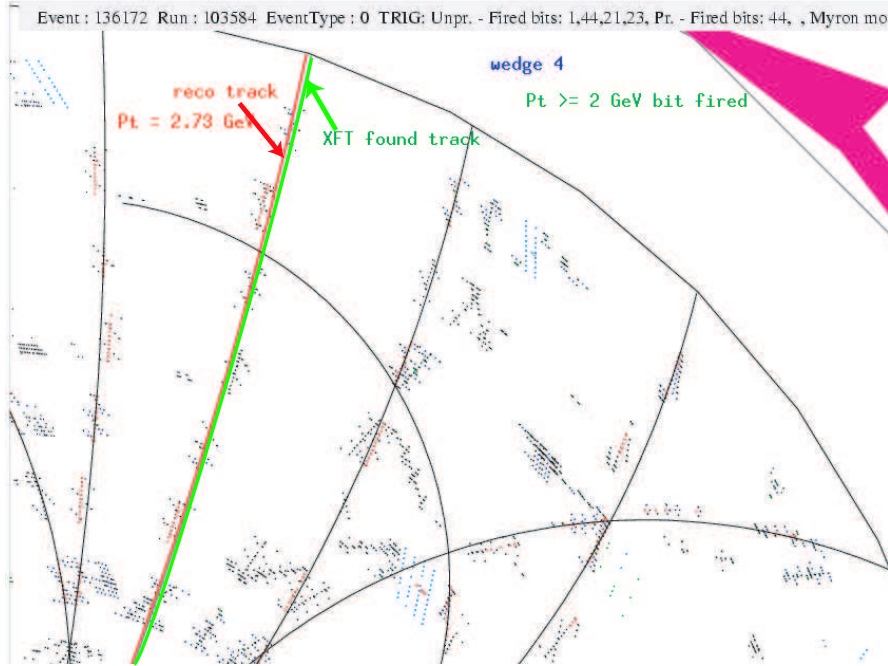


Figure 36: Event display showing an online XFT reconstructed COT track segment (green) compared with that obtained offline (red).

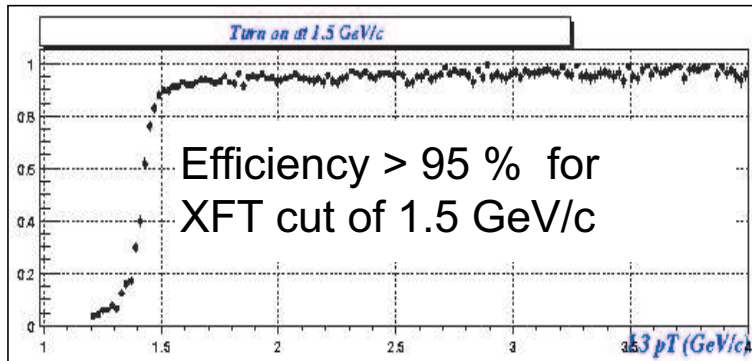


Figure 37: Efficiency of the XFT versus p_T of tracks.

(LSP) and R parity were violated or if it were the next to lightest supersymmetric particle (NLSP) and had a very narrow decay width to the LSP (possibly the gravitino). It is therefore interesting to search for evidence of a stable \tilde{t} (or any as yet unseen and possibly unexpected new charged particle for that matter) that lives long enough to traverse the entire CDF detector including the TOF before decaying. The \tilde{t} production rate [40] is mainly dependent upon $M_{\tilde{t}}$ and so an event count can be estimated for any integrated luminosity and mass. Such a study has been performed by CDF in 53 pb^{-1} of data and results in a mass limit in the range of ~ 95 (110) GeV for \tilde{t} embedded in a jet (or isolated in the detector) as seen in figure 42.



Figure 38: CDF lead project engineer R. Stanek inside the CDF solenoid during the installation of the TOF scintillator bars.

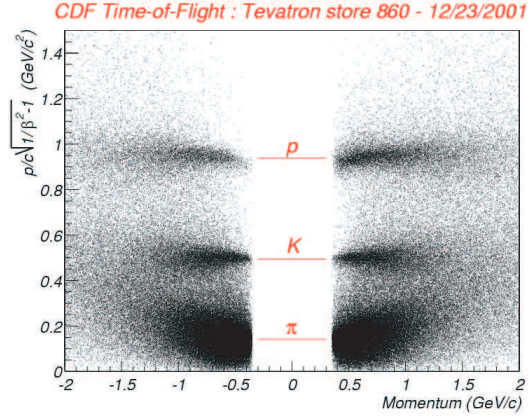


Figure 39: Early data from the TOF in Run 2 showing separation of p , K , and π at low transverse momentum.

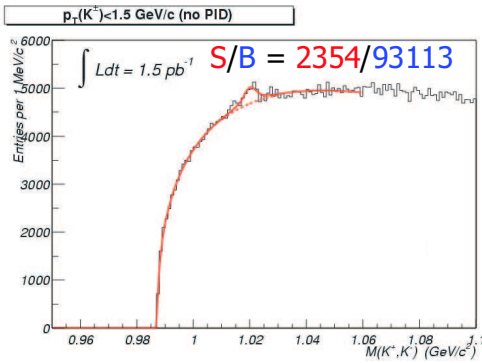


Figure 40: Invariant mass of K^+K^- candidate pairs as reconstructed without use of the TOF detector information.

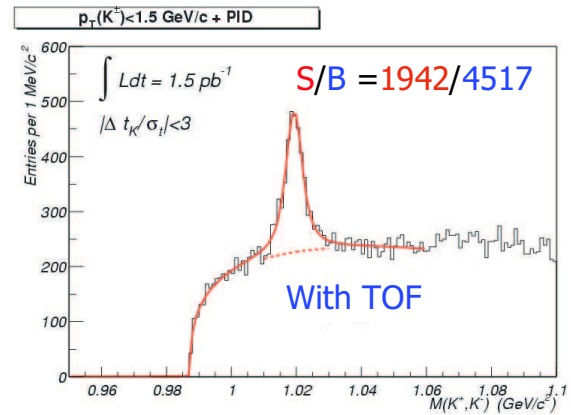


Figure 41: Invariant mass of K^+K^- candidate pairs after including the requirement that the tracks both be within 3σ of the expected flight time for Kaons as measured in the TOF.

The CDF silicon tracker [41] is made up of 3 subsystems containing only barrel layers as shown in figure 43. The silicon resides within the inner bore of the COT. There are a total of 7 silicon layers in the pseudorapidity range $|\eta| \lesssim 1.0$ and 8 layers in the forward region $1.0 \lesssim |\eta| \lesssim 1.9$. All layers are double-sided except the innermost one at a radius of ~ 1.5 cm. The double-sided layers have axial strips on one side and shallow stereo (1.2°)

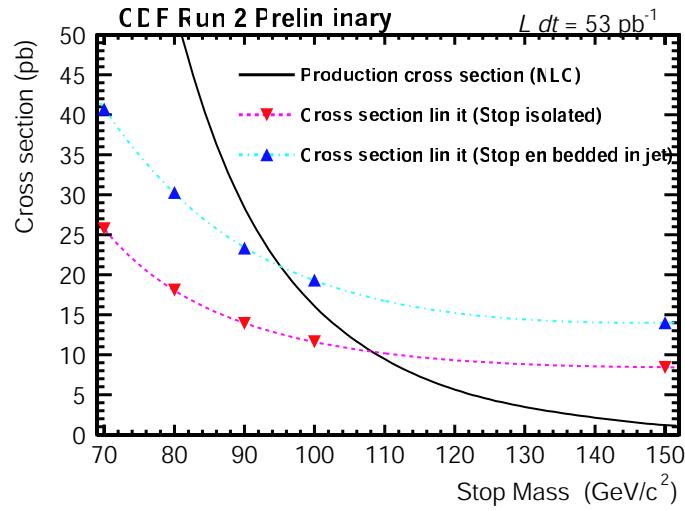


Figure 42: Recent preliminary CDF limits on the mass of a stable \tilde{t} either embedded in a jet or isolated in the detector.

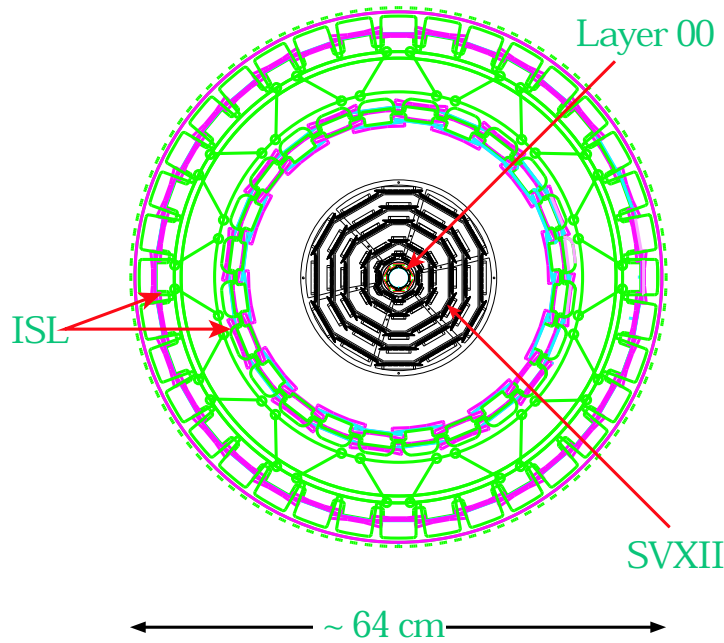


Figure 43: Drawing of the cross section of the cdf silicon subsystems as discussed in the text

or orthogonal stereo (90°) strips on the other side. The general characteristics of the CDF silicon are listed in table 7. The outermost system, called the Intermediate Silicon Layers (ISL) [42] is shown in figure 44.

The ISL provides track hit information with a resolution of $\sigma \sim 30 \mu m$ at large radii. This information is used in the central region to link track segments in the inner silicon

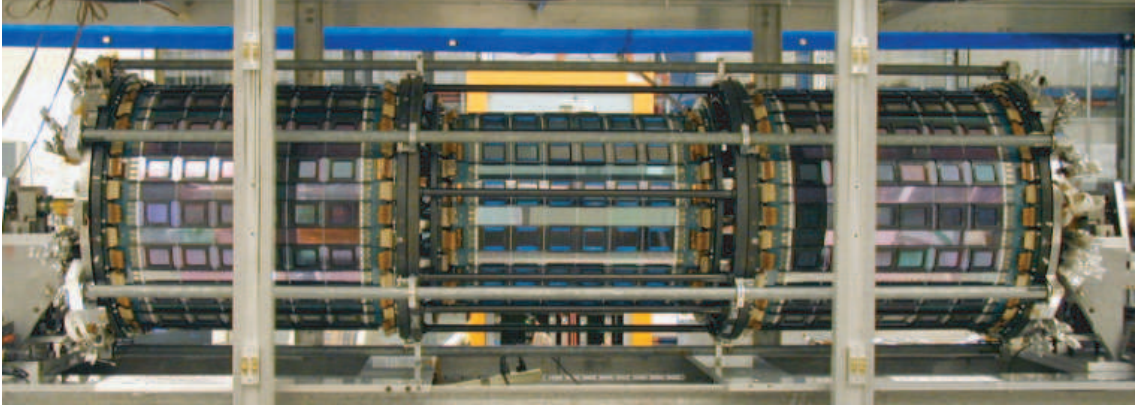


Figure 44: The CDF Intermediate Silicon Layers. This photograph was taken during construction of the detector at the FNAL Silicon Detector Center. The detector, which is roughly 2 m long, is shown in a large protective case from which the exterior side walls have been removed for visibility.

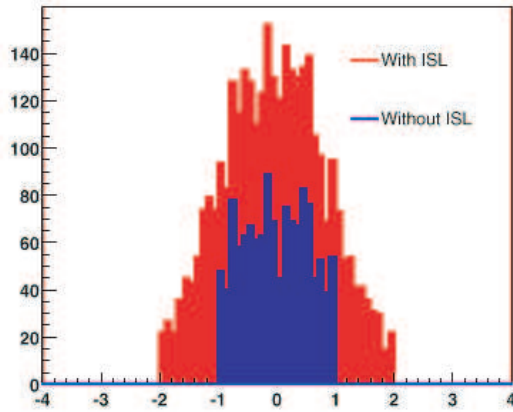


Figure 45: The impact of the ISL detector on the acceptance for trileptonic events is shown in this plot of the number of simulated events as a function of pseudorapidity η .

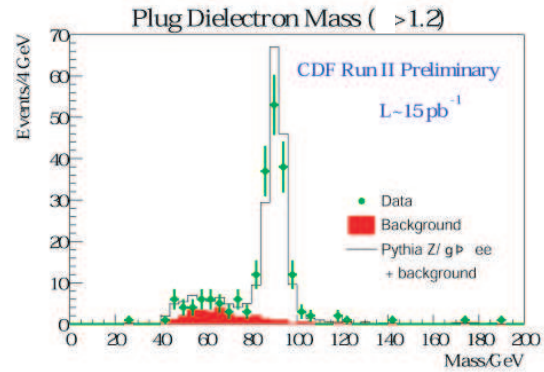


Figure 46: Reconstruction of the invariant mass of e^+e^- pairs in the end plug regions based on silicon-only tracking is shown.

layers to those in the COT. In the forward regions where the COT has little or no coverage, two ISL layers provide enough information to allow high purity tracking and well-resolved track parameters for forward lepton identification and forward b-tagging. Figure 45 shows the impact of the ISL on the trilepton searches discussed in section 1, while figure 46 shows the reconstruction of a $Z \rightarrow e^+e^-$ for electrons in the plug region using silicon-only information including hits from the ISL.

Inside the ISL is the SVXII detector [43]. The SVXII shown in figure 49 is arguably the most complex and compact silicon detector built to date. The main purpose of the SVXII is to provide pure track segments that can be combined with the COT segments to make tracks with very high resolution impact parameters in both the axial and stereo views. The SVXII construction was extremely difficult because of its compact and precise

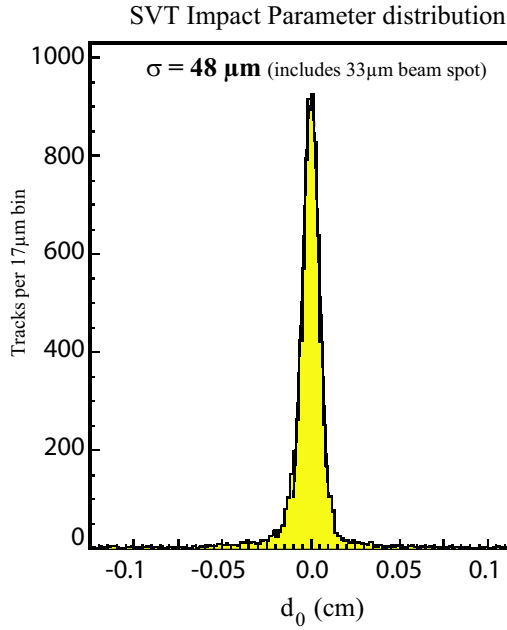


Figure 47: The online impact parameter distribution for SVT reconstructed tracks relative to the beam spot ($\sim 30 \mu m$). The SVT resolution is $\sim 40 \mu m$.

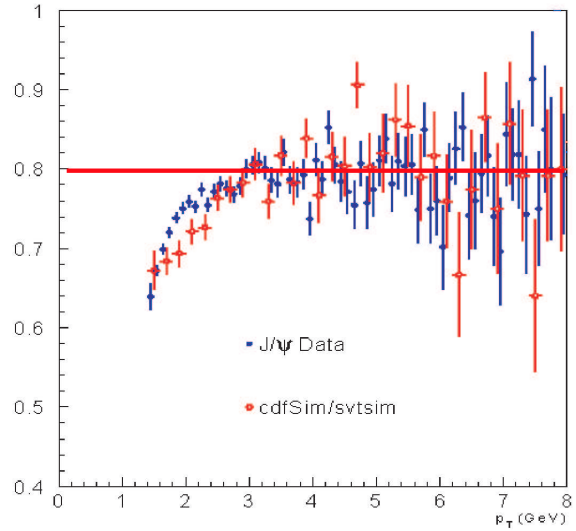


Figure 48: The track efficiency of the SVT as measured in $J/\psi \rightarrow \mu^+\mu^-$ events as a function of track p_T .

nature. Furthermore, the SVXII is used in an online Level 2 silicon vertexer trigger (SVT) [5] which uses COT track stubs to define roads in the silicon where it looks for axial hits to add to the tracks for higher resolution. The SVT is the first such trigger used in a hadron collider experiment and enables CDF to collect low E_T events with hadronic b decays for the first time. The online impact parameter distribution for tracks reconstructed with the SVT is shown in figure 47. The track efficiency of the SVT as a function of track p_T at the start of running was on the order of 80% as shown in figure 48 and is expected to rise to 90% with further improvements in operation of the silicon.

Inside the SVXII detector is the Layer 00 detector [44] which is shown in figure 50 during its installation. The Layer 00 detector is a very lightweight, fine-pitched microstrip detector at an average radius of 1.5 cm. The main purpose of the Layer 00 detector is to make it possible to obtain excellent impact parameter resolution down to $p_T \sim 300$ MeV.

The compact construction of the SVXII detector necessitated the presence of a fairly substantial amount of material in the tracking region. The material has been mapped with $\gamma \rightarrow ee$ conversions as shown in figure 51. The amount of material in the silicon region is substantially reduced in the design of the CDF

	Layer 00	SVXII	ISL
Si	1-sided	2-sided	2-sided
Stereo angles	-	$1.2^\circ, 90^\circ$	1.2°
Channels	13,824	405,504	303,104
Modules	48	360	296
Inner radius	1.35 cm	2.5	20
Outer radius	1.65 cm	10.6	28

Table 7: CDF silicon.

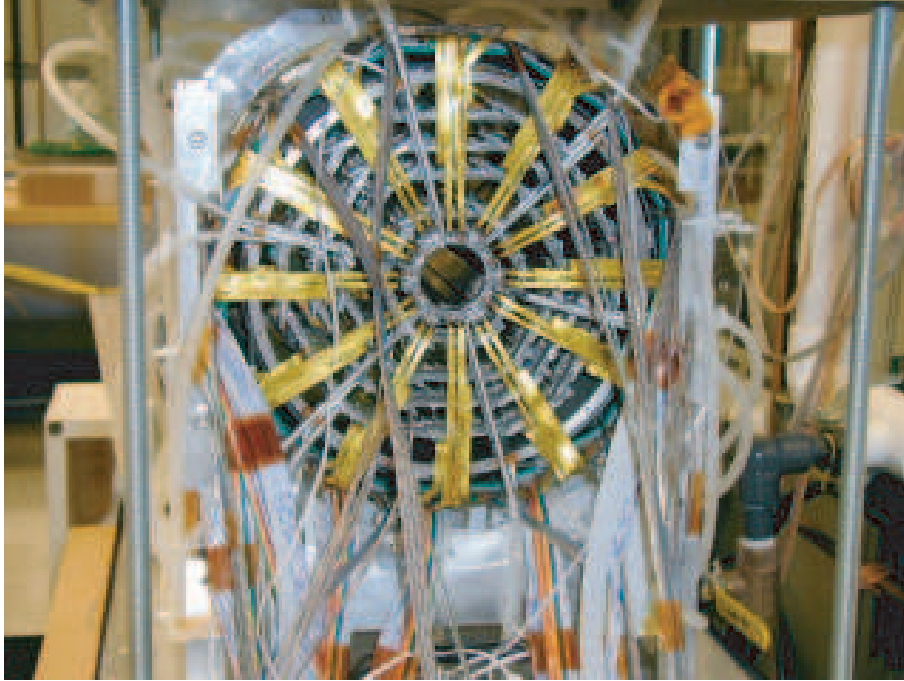


Figure 49: Photograph of one of three CDF SVXII detector barrels during construction.

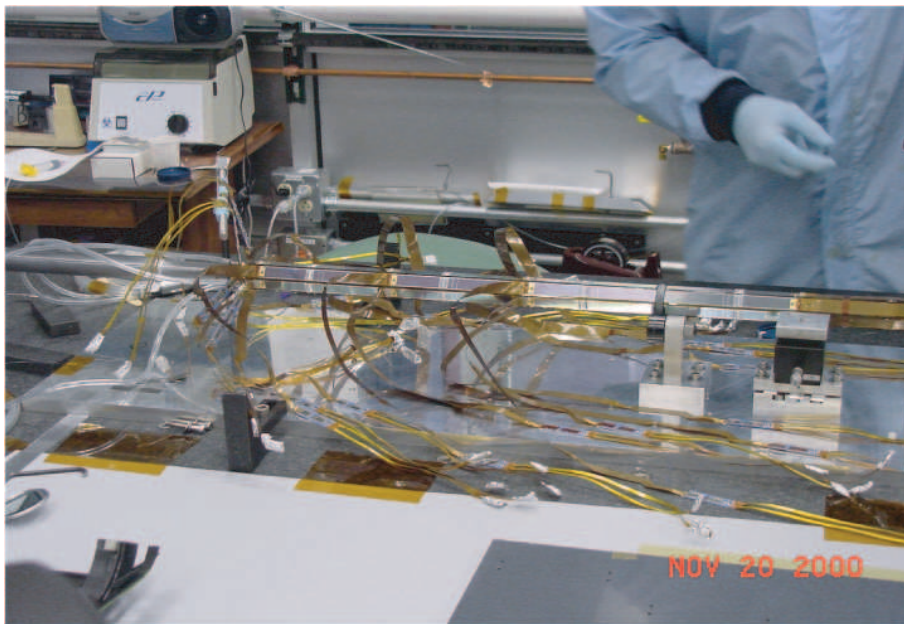


Figure 50: The CDF Layer 00 detector just after installation on the Beryllium beam pipe.

silicon upgrade for Run 2b [45].

4. Preliminary Run 2 Physics Results and Future Prospects

So where does the Tevatron collider program stand now on the path to finding the Higgs or

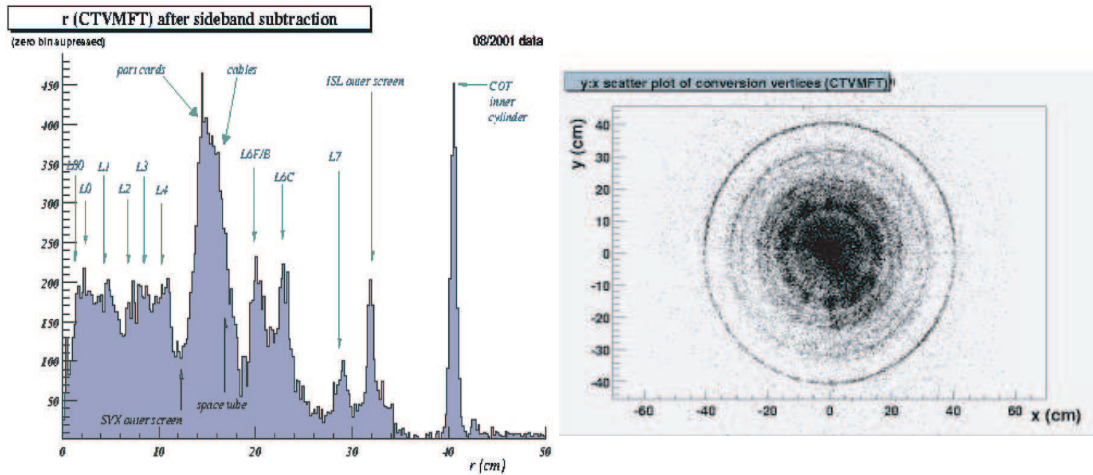


Figure 51: Photon conversions as a function of radius showing the relative amounts of material in the silicon.

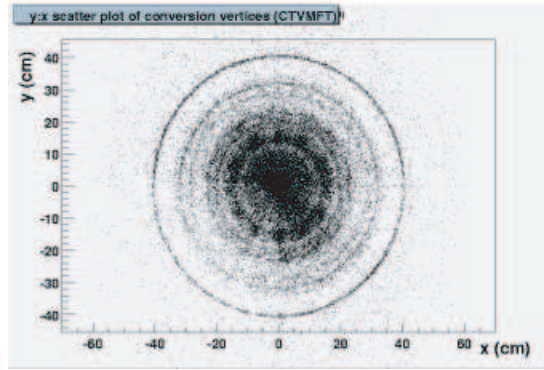


Figure 52: Scatter plot of photon conversions in the transverse plane showing the outlines of the various silicon layers and their electronics, supports, and services.

evidence for any of the new physics discussed earlier? These high stakes searches proceed along natural pathways that begin with more familiar Standard Model physics topics. As an example, the Higgs search begins with measurements of the W and Z boson cross sections. This is because the most prominent Standard Model (SM) Higgs signatures at the Tevatron are those involving Higgs produced in association with the vector bosons or decay of solo Higgs to a pair of W 's. It is therefore important to first have a detailed understanding of how the leptonic decays of the vector bosons are manifested in these experiments. Following closely behind the cross section measurements are studies of W or Z plus jets events. These events represent an important background to $t\bar{t}$ events as well as to Higgs, particularly at low mass where the dominant decay is $H \rightarrow b\bar{b}$. Once this effort is well underway, the next step is to look for evidence of b hadrons in the jets accompanying the vector bosons. The ability to tag b jets in such events is crucial to producing pure samples of $t\bar{t}$ events and to eliminating most of the background in $W + H \rightarrow l\nu + b\bar{b}$ events, leaving mainly the irreducible background $W + b\bar{b}$.⁴ Once b tagging is well understood, it is possible to begin to measure the cross section for $t\bar{t}$ in events containing W plus b jets. Finally, once the top analysis is reasonably stable and well understood, one is in a good position to search for a low mass SM Higgs. Of course, a significant amount of data is required to test SM expectations. Nevertheless, new *experimental* limits can be set with smaller quantities of data and there's even the possibility that something may turn up that the theorists did not expect.

Currently CDF and D0 have begun to present W and Z cross sections as well as preliminary cross sections for $t\bar{t}$ production. In addition, b tagging algorithms are becoming well enough understood to be used with confidence. Both experiments have collected data

⁴Of course given the roughly 20% efficiency expected for tagging of c jets, $W + c\bar{c}$ events will also contribute to the irreducible backgrounds for Higgs.

samples enriched in $t\bar{t}$ events in their W plus b jets samples.

With regard to searches for new physics, the analysis path again begins with W and Z studies. In the search for new particles, lepton (particularly e and μ) identification is important in the forward regions of the detector as discussed above in relation to figure 45. In early data-taking the analyses for which forward leptons are crucial are the W and Z asymmetries. These measurements are currently well underway. The next step is to study W or Z plus b or c jets. Here CDF benefits from the SVT displaced track trigger to collect large samples of hadronic b and c meson and baryon decays. The next step in the analysis path is to measure the $t\bar{t}$ cross section in the dilepton channel. Finally, once this measurement is well understood, there is adequate confidence in the identification of the relevant objects to begin searching for new physics with leptons, photons, b or c tags, and possibly large missing E_T and jets.

4.1 W and Z Studies

As of March 2003, CDF and D0 have collected substantial samples of W and Z events. Figure 53 shows the transverse mass of over 38,000 $W \rightarrow e\nu$ candidates in CDF from which one obtains the preliminary measurement: $\sigma \cdot Br = 2.64 \pm 0.01(stat) \pm 0.09(syst) \pm 0.15(luminosity) nb$ [46]. The missing E_T resolution in Run 2 compares well to that of Run 1 as shown in figure 54.

Figure 55 shows the distribution of $Z \rightarrow e^+e^-$ as measured in the D0 experiment [47]. The CDF and D0 experiments have preliminary Run 2 measurements of the W and Z production rates and widths and their ratios⁵. The results for CDF are presented in table 8. D0 has performed a search for a high mass Z' boson by searching for an excess in the full spectrum of Z and Drell-Yan production of opposite-sign lepton pairs. Figure 56 shows the D0 e^+e^- invariant mass distribution for 50pb^{-1} . A simulated 600 GeV Z' peak at ten times the theoretical cross section is superimposed. The e^+e^- data alone imply that such a Z' must lie below a mass of ~ 625 GeV.

Measurement	CDF Run 2 preliminary	PDG or Theory
$\sigma Br(W \rightarrow e\nu)$	$2.64 \pm 0.01 \pm 0.09(sys) \pm 0.15(lum) nb$	$2.69 \pm 0.10 nb$ (NNLO)
$\sigma Br(W \rightarrow \mu\nu)$	$2.64 \pm 0.02 \pm 0.12(sys) \pm 0.16(lum) nb$	“ “
$\sigma Br(W \rightarrow \tau\nu)$	$2.62 \pm 0.07 \pm 0.21(sys) \pm 0.16(lum) nb$	“ “
$\frac{Br(W \rightarrow \tau\nu)}{Br(W \rightarrow e\nu)}$	$0.99 \pm 0.04 \pm 0.07(sys)$	
$g(\tau)/g(e)$	$0.99 \pm 0.02 \pm 0.04(sys)$	
$\sigma Br(Z \rightarrow ee)$	$267 \pm 6.3 \pm 15.2(sys) \pm 15.5(lum) pb$	$250.2 pb$ (NNLO)
$\sigma Br(Z \rightarrow \mu\mu)$	$246 \pm 6 \pm 12(syst) \pm 15(lum) pb$	“ “
$\frac{\sigma(W \rightarrow e\nu)}{\sigma(Z \rightarrow ee)}$	$9.88 \pm 0.24 \pm 0.47(sys)$	
$\frac{\sigma(W \rightarrow \mu\nu)}{\sigma(Z \rightarrow \mu\mu)}$	$10.69 \pm 0.27 \pm 0.33(sys)$	
Extracted Γ_W	$2.11 \pm 0.05 \pm 0.07(syst) \pm 0.02(ext) GeV$	$2.118 \pm 0.042 GeV$ (PDG)

Table 8: CDF W and Z measurements for a total integrated luminosity of 72 pb^{-1} .

⁵D0 results are available for $10\text{-}15 \text{ pb}^{-1}$ [47] and updated results will be released imminently.

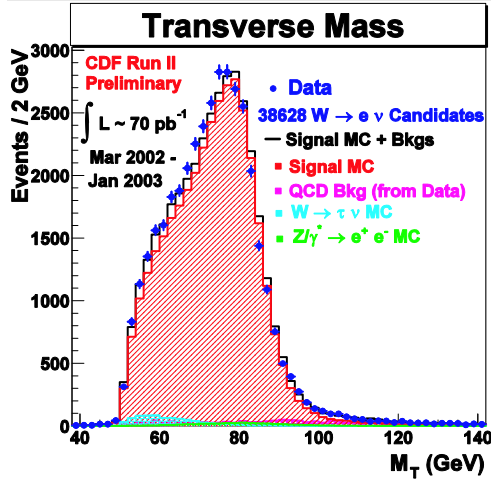


Figure 53: Transverse mass (M_T) of CDF $W \rightarrow e\nu$ candidates in Run 2.

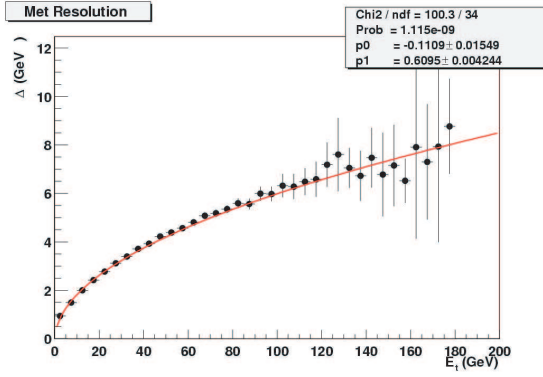


Figure 54: Resolution of missing E_T in CDF as a function of missing E_T .

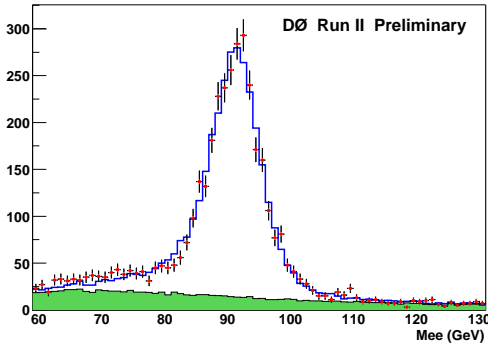


Figure 55: The D0 e^+e^- invariant mass distribution for 50 pb^{-1} is shown.

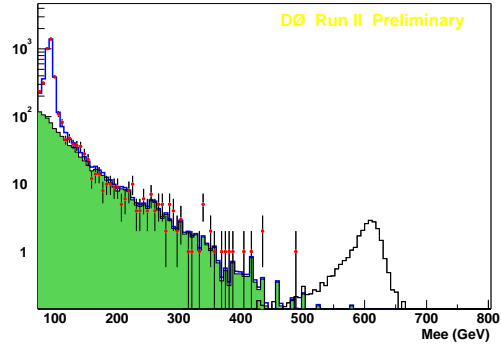


Figure 56: The full D0 e^+e^- mass spectrum in Run 2 with a 600 GeV Z' signal superimposed at ten times estimated cross section.

The CDF data for the forward-backward charge asymmetry of e^+e^- pairs (A_{fb}^e) is shown in figure 57. This asymmetry results from the fact that the reaction $p\bar{p} \rightarrow l^+l^-$ is mediated both by virtual photons at low values of $M_{l^+l^-}$ [48], by the Z at $M_{l^+l^-} \sim M_Z$, and by both processes, including interference, at all other masses. At tree level the angular differential cross section in the center of mass frame is:

$$\frac{d\sigma(q\bar{q} \rightarrow Z/\gamma \rightarrow l^+l^-)}{d\cos\theta} = A(1 + \cos^2\theta) + B\cos\theta$$

CDF is also in the process of re-measuring the forward-backward charge asymmetry in leptonic decays of W s. Here the asymmetry arises from the differences in the parton density functions of the proton for d and u quarks. It was shown in Run 1 that this measurement is extremely powerful for constraining empirical models of proton structure [50]. The additional lepton coverage provided by the new CDF and D0 tracking detectors greatly enhances the discrimination of various parton distribution functions [51]. The sensitivity

of the channel $W \rightarrow e\nu$ alone will be comparable to that of both the e and μ channels in Run 1 and will extend to larger values of lepton rapidity, as seen in figure 58.

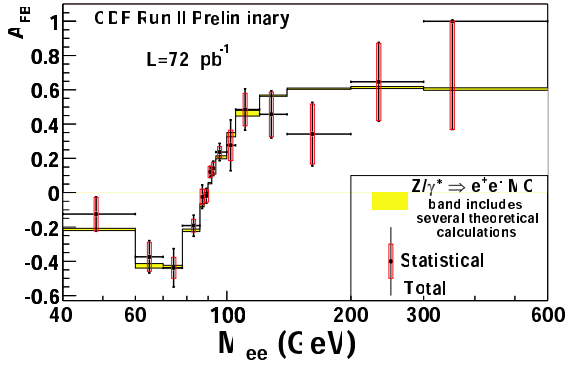


Figure 57: Preliminary measurement of forward-backward asymmetry in $Z \rightarrow ee$ events by CDF in Run 2.

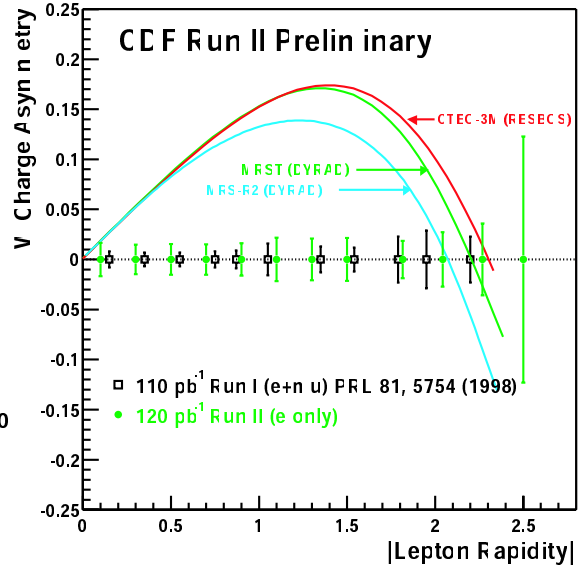


Figure 58: The expected uncertainties on the W charge asymmetry with 120 pb^{-1} of $W \rightarrow e\nu$ data are plotted on axis and compared to the uncertainties in Run 1 for both $e\nu$ and $\mu\nu$ channels combined. The asymmetries for various partonic models of the proton are also plotted.

4.2 Top Physics

The CDF and D0 experiments have now collected enough data in Run 2 to begin to measure top quark production properties. Groups are also actively working on new measurements of kinematics including the mass of the top quark. As mentioned above, top is an excellent stepping stone on the path to new physics since a good understanding of top events requires such a high level of knowledge of how

leptons, jets, long-lived b hadrons, and neutrinos are manifested in one's detector. Top physics is of course also quite important on its own. The top quark is extremely massive, and has an extremely short lifetime of order 10^{-24} s. This means that the top quark will decay before hadronization making it the only quark whose free decay can be studied. The Tevatron experiments plan a very broad program of study in the realm of top physics [52]. Projections for top production in 2 fb^{-1} (Run 2a) are listed in table 9.

	Run 1	Run 2a
CM Energy [TeV]	1.8	1.96
Integrated Luminosity [fb^{-1}]	0.1	2.0
$\sigma_{t\bar{t}}$ [pb]	5.0	7.0
$\sigma(\text{single top})$ [pb]	2.5	3.4
$N_{t\bar{t}}$ produced	500	14,000
Single top	250	6,800
$N(t\bar{t} \rightarrow l^+l^-)$	4	150
$N(t\bar{t} \rightarrow l^+ \geq 3 \text{ jets})$	30	2000

Table 9: Top quark production in Run 1 compared with projections for 2 fb^{-1} in Run 2a.

CDF and D0 have made preliminary measurements of $\sigma_{t\bar{t}}$ and M_t in several decay channels as shown in table 10. The combined D0 and CDF top quark mass measurement for Run 1 was $M_t = 174.3 \pm 5.1$ GeV. Recently D0 has re-optimised their measurement of M_t in Run 1 and has obtained a new preliminary result of 179.9 ± 3.6 (*stat*) ± 6.0 (*syst*) GeV in which the statistical error has been reduced substantially [54]. Current measurements of the mass are not yet competitive with those of Run 1 as they are still being refined, and also entail less data (~ 70 versus ~ 110 pb⁻¹).

	D0	CDF
$\sigma_{t\bar{t}}$ Dileptons [pb]		$13.2 \pm 5.9 \pm 1.5$ (<i>sys</i>)
$\sigma_{t\bar{t}}$ Lepton + jets [pb]		$5.3 \pm 1.9 \pm 0.8$ (<i>sys</i>)
$\sigma_{t\bar{t}}$ Both Channels [pb]	$8.4^{+1.9}_{-3.7}$ (<i>stat</i>) $^{+5.0}_{-3.5}$ (<i>syst</i>) ± 0.8 (<i>lum</i>)	
M_t (Lepton + jets) [GeV]		$171.2 \pm 13.4 \pm 9.9$ (<i>sys</i>)

Table 10: Preliminary Run 2 measurements in $t\bar{t}$ production.

4.3 CDF's Surprising Charm (and Bottom).

As mentioned in my earlier discussion of the CDF upgrades, one of the more exciting new additions to CDF is the SVT silicon tracker and trigger. This trigger was designed to allow CDF to collect events with hadronic b decays at low E_T . Previously in Run 1, one had to rely on at least one b hadron decaying semileptonically (to e or μ) in order to discriminate from the huge dijet backgrounds present at the Tevatron. The new trigger was quite a difficult endeavor and there was some skepticism about how well it would perform - particularly since it relied on so many other things being done correctly like the extremely precise construction and final alignment of the silicon detector to the beam line.

From the start of Run 2 the SVT has operated extremely well and CDF has indeed accumulated new types of data. A pleasant surprise, but of course not at all surprising in retrospect, is the fact that CDF has accumulated huge samples of hadronic charm decays with the SVT as well as hadronic bottom decays. The former led to a measurement of the difference in mass of the D_s^\pm and the D^\pm as one of the earliest CDF results in Run 2 [55]. CDF finds

$$m(D_s^+) - m(D^+) = 99.41 \pm 0.38$$
 (*stat*) ± 0.21 (*syst*) MeV

This is to be compared with the current PDG value of 99.2 ± 0.5 MeV. Figure 59 shows the D_s^+ and D^+ peaks in CDF data.

Samples of reconstructed hadronic b hadrons are more difficult to obtain since there are in general more daughter particles involved in the decays and hence detector inefficiencies become greatly magnified. In addition, CDF silicon detectors were installed but not fully commissioned at the start of data taking and so it took quite a long time to bring them up to optimal efficiency [56].

There are many important direct measurements planned for the low E_T charm and bottom samples that will be collected by CDF in Run 2. The relevance of these samples to

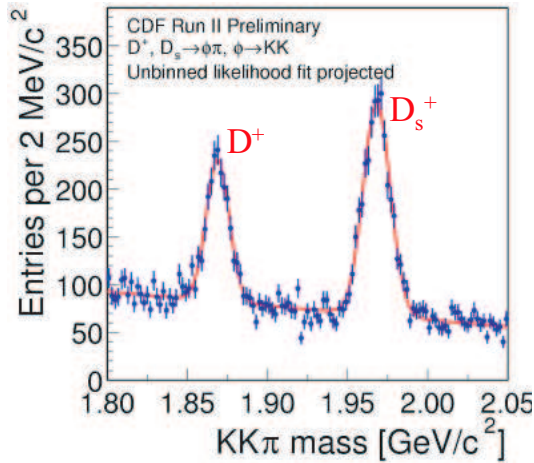


Figure 59: The CDF reconstruction of D_s^+ and D^+ .

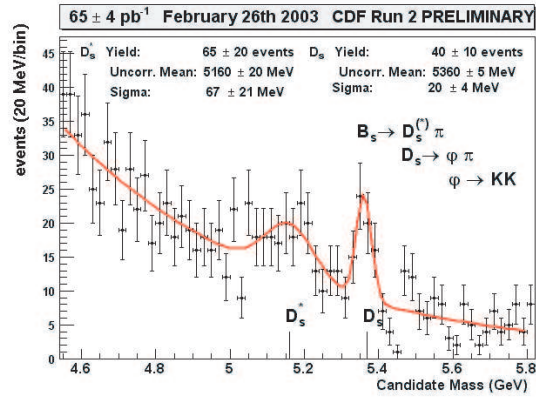


Figure 60: An example of the full reconstruction of hadronic b decays in CDF is provided by this mass spectrum with peaks observed for $B_s \rightarrow D_s^* \pi$ and $B_s \rightarrow D_s \pi$.

high E_T physics stems from the fact that they will allow CDF to study b and c jet tagging directly in data containing enriched samples of hadronic decays. Previously, systematic studies of b tagging for instance were confined to inclusive lepton samples and Monte Carlo [57].

5. Summary and Conclusions

The CDF and D0 detectors have undergone extensive multi-year upgrades to take advantage of the opportunities presented by the similarly upgraded Fermilab accelerator complex. After a difficult start, most detector subsystems are now performing at or beyond design specifications while a small number will probably never quite achieve their design goals. The Tevatron has itself struggled and has not managed to integrate luminosity at the level expected. However, work has continued and progress is steadily being made to understand the problems the accelerator is having. New instantaneous luminosity records are regularly being established.

The physics program is now well underway. New results for W and Z production and for t , b , and c quark physics have been presented with special attention given to new capabilities and future expectations. While data has been slow to accumulate at the Tevatron, it is nevertheless clear from these results that the CDF and D0 collaborations are making great progress in understanding and operating their detectors, and in developing new techniques and analyses to take advantage of new capabilities available in Run 2.

How much can actually be achieved by the Tevatron program in the future depends on many things. The biggest concern at present is the performance of the accelerator. It is hoped that it will improve significantly in coming years. It is certainly true that the Fermilab director and management are making this a top priority. Without such an improvement, the high E_T physics program will be more limited but still important. With

only 1 fb^{-1} of new data, which could be obtained before the start of the Large Hadron Collider operation at CERN by very modest improvements in luminosity or consistency of operation of the accelerator complex, it will be possible to make substantial improvements in top quark, and W/Z studies. Some, albeit limited new constraints on SUSY and SM Higgs would also be possible. With a bit better performance, as may very well be provided by the recycler, it may be possible to integrate $\sim 5 \text{ fb}^{-1}$ of data per experiment. At this level, we may rule out a low mass SM Higgs for instance, and come quite close to ruling out the Minimal SUSY Model. More constraints on SUSY and other new particles via direct searches will be attainable. In fact this statement remains true with increased integrated luminosity up to levels that are well beyond what can be achieved in the pre-LHC era. Where it really hurts to fall short of our goal of $\sim 10 - 15 \text{ fb}^{-1}$ per experiment is in the realm of a Higgs *discovery*. While it is possible to rule out the Higgs with less data, it is not likely we can claim any kind of observation should it be present. It is therefore probable, barring a major new delay in the LHC project, that the FNAL Tevatron will join the list of illustrious facilities that had hoped to find the Higgs but could not do so.

In summary, though a Higgs discovery may be far from assured, the Tevatron program will very certainly be able to generate new results of major importance at each new step in integrated luminosity from now until the time when the LHC experiments start to produce results.

Acknowledgments

I thank A. Affolder, F. Bedeschi, C.S. Hill, C. Mills, D. Stuart, J. Womersley, and the many members of CDF and D0 who assisted me in preparing this note. I also thank my wife Helen for putting up with me in general and for proof-reading this note in particular. Finally, I would also like to thank the organizers of the 26th John's Hopkins Workshop for their wonderful hospitality and a marvelous workshop.

JHW2002/013

References

- [1] The LEP Electroweak Working Group, public page:
<http://lepewwg.web.cern.ch/LEPEWWG/>
- [2] M. S. Chanowitz *Phys. Rev. D* **66** (2002) 073002
- [3] M. Carena, J. S. Conway, H. E. Haber, J. D. Hobbs, et al [hep-ph/0010338](#)
- [4] S. Kuhlmann (for the CDF collaboration) *Int. J. Mod. Phys. A* **16S1A** (2001) 255
- [5] W. Ashmanskas (for the CDF collaboration) *Nucl. Instrum. Meth.* **A447** (2000) 218
- [6] W. Taylor (for the D0 collaboration) *IEEE Trans. Nucl. Sci.* **48** (2001) 557
- [7] B. H. Denby FERMILAB-CONF-92-121, April 1992
- [8] J. Conway private communication.
- [9] C. Haber, J. Incandela et al. Report of the CDF Run 2b silicon working group:
<http://www-cdf.fnal.gov/run2b/>
- [10] J. Campbell [hep-ph/0204093](#)
- [11] J. Goldstein et al. *Phys. Rev. Lett.* **86** (2001) 1694;
J. Incandela Higgs workshop, FNAL, May 5 2001 <http://conferences.fnal.gov/higgsworkshop/>
- [12] J. F. Gunion, et al.; *The Higgs Hunter's Guide*, (Addison-Wesley; Redwood City), 1990.
- [13] S. Dawson [hep-ph/9411325](#)
- [14] S. Abel et. al [hep-ph/0003154](#)
- [15] R. Demina et al. [hep-ph/9910275](#)
- [16] N. Arkani-Hamed, S. Dimopoulos, and G.R. Dvali *Phys. Lett. B* **429** (1998) ,263
- [17] L. Randall and R. Sundrum *Phys. Rev. Lett.* **83** (1999) 3370
- [18] C.D. Hoyle et al. *Phys. Rev. Lett.* **86** (2001) 1418
- [19] J. C. Long and J. C. Price [hep-ph/0303057](#)
- [20] B. Abbott et al. *Phys. Rev. Lett.* **86** (2001) 1156
- [21] D. Acosta et al. *Phys. Rev. Lett.* **89** (2002) 281801
- [22] A. Hewett and M. Spiropulu *Ann. Rev. Nucl. Part. Sci.* **52** (2002) 397
- [23] J. Incandela *Nucl. Instrum. Meth.* **A453** (2000) 17
- [24] CDF and D0 collaborations, submitted to *Phys. Rev. D* (2003) .
- [25] D. Glenzinski (for the CDF collaboration) [hep-ex/0211038](#)
- [26] Fermilab Beams Division <http://www-bd.fnal.gov/>
- [27] S. D. Holmes et al. *Part. Accel.* **26** (1990) 193
- [28] G. Jackson, FERMILAB-TM-1991, Nov. 1996
- [29] Fermilab Beams Division luminosity page
<http://www-bdnew.fnal.gov/operations/lum/lum.html>
- [30] V. Buscher et al. *Int. J. Mod. Phys. A* **16S1C** (2001) 1068

- [31] R. Lipton (for the D0 collaboration) *Nucl. Instrum. Meth.* **A418** (1998) 85
- [32] M. Narain (for the D0 collaboration) *Nucl. Instrum. Meth.* **A447** (2000) 223
- [33] M. R. Wayne (for the D0 collaboration) *Nucl. Instrum. Meth.* **A387** (1997) 278
- [34] G. C. Blazey (for the D0 collaboration) FERMILAB-CONF-97-395-E, Nov. 1997
- [35] The CDF II Detector Technical Design Report
<http://www-cdf.fnal.gov/upgrades/tdr/tdr.html>
- [36] K. Burkett (for the CDF collaboration) *Nucl. Instrum. Meth.* **A461** (2001) 62;
 K. T. Pitts (for the CDF collaboration) *Nucl. Phys.* **61B** (Proc. Suppl.) (1998) 230
- [37] F. Bedeschi et. al *Nucl. Instrum. Meth.* **A268** (1988) 50
- [38] W. Ashmaskas (for the CDF collaboration) *Nucl. Instrum. Meth.* **A447** (2000) 218
- [39] C. Grozis et al. *Int. J. Mod. Phys. A* **16S1C** (2001) 1119;
 C. Grozis et al. *Nucl. Phys.* **93** (Proc. Suppl.) (2001) 344
- [40] W. Beenakker et al. *Nucl. Phys.* **B 515** (1998) 3;
 E. Berger et al. *Phys. Rev.* **D 59** (1999) 074024
- [41] P. Merkel (for CDF the collaboration) *Nucl. Instrum. Meth.* **A501** (2003) 1;
 A. Sill (for the CDF collaboration) *Nucl. Instrum. Meth.* **A447** (2000) 1
- [42] A. Affolder (for the CDF collaboration) *Nucl. Instrum. Meth.* **A453** (2000) 84
- [43] J. Antos et. al *Nucl. Instrum. Meth.* **A383** (1996) 13
- [44] C. Hill (for the CDF collaboration) FERMILAB-CONF-03-029-E, March 2003;
 T. K. Nelson (for the CDF collaboration) *Int. J. Mod. Phys. A* **16S1C** (2001) 1091
- [45] S. Cabrera (for CDF the collaboration) FERMILAB-CONF-02-164-E, August 2002;
- [46] P. Koehn (for the CDF collaboration) XXXVIIIth Rencontres de Moriond, March 2003
- [47] T. Diehl (for the D0 collaboration) XXXVIIIth Rencontres de Moriond, March 2003
<http://www-d0.fnal.gov/Run2Physics/wz>
- [48] S. D. Drell and T. M. Yan *Phys. Rev. Lett.* **25** (1970) 316
- [49] K. Hagiwara et al. (Particle Data Group) *Phys. Rev.* **D 66** (2002) 010001
- [50] F. Abe et al. (the CDF Collaboration) *Phys. Rev. Lett.* **81** (1998) 5754
- [51] C. Issever (for the CDF collaboration) `hep-ex/0301002`.
- [52] Report of the TeV 2000 Working Group <http://theory.fnal.gov/TeV2000.html> May 1996
- [53] L. Demortier et al. (For the CDF and D0 collaborations) FERMILAB-TM-2084
- [54] J. Estrada (for the D0 collaboration) `hep-ex/0302031` Feb. 2003
- [55] Measurement of ... $m(D_s^+) - m(D^+)$ at CDF II, submitted to *Phys. Rev.* **D** (2003) .
 A. Korn (for the CDF collaboration) XXXVIIIth Rencontres de Moriond, March 2003
- [56] S. Nahn (for the CDF collaboration) Fermilab-Conf-03-055-E
- [57] See for instance F. Abe et al (The CDF Collaboration) *Phys. Rev.* **D 50** (1994) 2966